

AWARD NUMBER: W81XWH-16-1-0206

TITLE: Targeting Androgen Receptor-Bypass Mechanisms to Enhance Prostate Cancer Therapy

PRINCIPAL INVESTIGATOR: Michael D. Nyquist, PhD

CONTRACTING ORGANIZATION: Fred Hutchison Cancer Research Center  
Seattle, WA 98109

REPORT DATE: October 2018

TYPE OF REPORT: Final

PREPARED FOR: U.S. Army Medical Research and Materiel Command  
Fort Detrick, Maryland 21702-5012

DISTRIBUTION STATEMENT: Approved for Public Release;  
Distribution Unlimited

The views, opinions and/or findings contained in this report are those of the author(s) and should not be construed as an official Department of the Army position, policy or decision unless so designated by other documentation.

# REPORT DOCUMENTATION PAGE

Form Approved  
OMB No. 0704-0188

Public reporting burden for this collection of information is estimated to average 1 hour per response, including the time for reviewing instructions, searching existing data sources, gathering and maintaining the data needed, and completing and reviewing this collection of information. Send comments regarding this burden estimate or any other aspect of this collection of information, including suggestions for reducing this burden to Department of Defense, Washington Headquarters Services, Directorate for Information Operations and Reports (0704-0188), 1215 Jefferson Davis Highway, Suite 1204, Arlington, VA 22202-4302. Respondents should be aware that notwithstanding any other provision of law, no person shall be subject to any penalty for failing to comply with a collection of information if it does not display a currently valid OMB control number. **PLEASE DO NOT RETURN YOUR FORM TO THE ABOVE ADDRESS.**

<b>1. REPORT DATE</b> October 2018	<b>2. REPORT TYPE</b> Final	<b>3. DATES COVERED</b> 1 Jul 2016 - 30 Jun 2018
---------------------------------------	--------------------------------	---

<b>4. TITLE AND SUBTITLE</b>  Targeting Androgen Receptor-Bypass Mechanisms to Enhance Prostate Cancer Therapy	<b>5a. CONTRACT NUMBER</b>
	<b>5b. GRANT NUMBER</b> W81XWH-16-1-0206
	<b>5c. PROGRAM ELEMENT NUMBER</b>

<b>6. AUTHOR(S)</b>  Michael D. Nyquist	<b>5d. PROJECT NUMBER</b>
	<b>5e. TASK NUMBER</b>
	<b>5f. WORK UNIT NUMBER</b>

<b>7. PERFORMING ORGANIZATION NAME(S) AND ADDRESS(ES)</b>  FRED HUTCHINSON CANCER RESEARCH CENTER 1100 FAIRVIEW AVE N SEATTLE WA 98109-443	<b>8. PERFORMING ORGANIZATION REPORT NUMBER</b>
--	---

<b>9. SPONSORING / MONITORING AGENCY NAME(S) AND ADDRESS(ES)</b>  U.S. Army Medical Research and Materiel Command Fort Detrick, Maryland 21702-5012	<b>10. SPONSOR/MONITOR'S ACRONYM(S)</b>
	<b>11. SPONSOR/MONITOR'S REPORT NUMBER(S)</b>

**12. DISTRIBUTION / AVAILABILITY STATEMENT**  
Approved for Public Release; Distribution Unlimited

**13. SUPPLEMENTARY NOTES**

**14. ABSTRACT**  
DNPC prostate cancers that evolve as a direct result of increased selective pressures to bypass AR signaling are of increasing importance and likely represent the next major challenge for the treatment of prostate cancer. Autocrine and paracrine FGF pathway activation can bypass AR dependence and targeting the FGF and MAPK pathways can repress AR-null prostate cancer. We further found that TP53 and RB1 play a role in uncoupling the prostate cancer cell from control of androgen through dysregulation of cell cycle. However, dual loss of TP53 and RB1 is insufficient to mediate a full transition to DNPC. Finally, we identified an additional therapeutic approach to DNPC thought targeting DNMT though the inhibitor SGI1027.

**15. SUBJECT TERMS**  
prostate cancer, castration resistance, bypass pathways, androgen receptor, endocrine uncoupling, tumor suppressor, TP53, RB1, CRISPR/CAS9, drug screening, androgen independence

<b>16. SECURITY CLASSIFICATION OF:</b>			<b>17. LIMITATION OF ABSTRACT</b>  Unclassified	<b>18. NUMBER OF PAGES</b>  34	<b>19a. NAME OF RESPONSIBLE PERSON</b> USAMRMC
<b>a. REPORT</b>  Unclassified	<b>b. ABSTRACT</b>  Unclassified	<b>c. THIS PAGE</b>  Unclassified			<b>19b. TELEPHONE NUMBER</b> (include area code)

## Table of Contents

	Page
<b>1. Introduction.....</b>	<b>4</b>
<b>2. Keywords.....</b>	<b>4</b>
<b>3. Accomplishments.....</b>	<b>4-10</b>
<b>4. Impact.....</b>	<b>10</b>
<b>5. Changes/Problems.....</b>	<b>11</b>
<b>6. Products, Inventions, Patent Applications, and/or Licenses.....</b>	<b>11</b>
<b>7. Participants &amp; Other Collaborating Organizations.....</b>	<b>11</b>
<b>8. Special Reporting Requirements.....</b>	<b>11</b>
<b>9. Appendices.....</b>	<b>11-34</b>

## INTRODUCTION:

Prostate cancer is the second leading cause of male cancer deaths in the United States. The frontline treatment for metastatic prostate cancer is androgen deprivation therapy (ADT), which seeks to eliminate Androgen Receptor (AR) transcriptional activity. Currently, AR-null prostate cancers, such as AR-null/non-neuroendocrine or double-negative prostate cancer (DNPC), are a minority of cases. However, as therapies that target AR signaling become more and more effective, DNPC prostate cancers that evolve as a direct result of increased selective pressures to bypass AR signaling are of increasing importance and likely represent the next major challenge for the treatment of prostate cancer.

Tumor suppressor loss, especially TP53 and RB1, are strongly associated with castration resistance and transdifferentiation to AR-null or neuroendocrine (NE) phenotypes<sup>1,2</sup>. In support of this, TP53 and Rb1 loss in murine models of PC promotes tumor plasticity and acquisition of neuroendocrine-like features<sup>3,4</sup>. A recently published study found that loss of differentiation to a more “plastic” state and antiandrogen resistance can be induced by expression of TP53 and RB1 shRNAs in human prostate cancer cell lines via SOX2 upregulation<sup>5</sup>. Therefore, dual loss of TP53 and RB1 is a plausible mechanism of progress to DNPC.

**KEYWORDS:** Prostate Cancer, Castration resistance, bypass pathways, androgen receptor, endocrine uncoupling, tumor suppressor, TP53, RB1, CRISPR/CAS9, Drug screening, androgen independence

## ACCOMPLISHMENTS:

### Major Project Goals:

*Aim 1: Identify cell survival and growth-promoting mechanisms that are active in human castration-resistant ‘double negative’ prostate cancers devoid of AR activity*

*Aim 2: Utilize genome-wide screening approaches to define signaling pathways capable of sustaining AR-null prostate cancer growth.*

*Aim 3: Determine whether genetic and pharmacological inhibition of AR-bypass pathways can induce apoptotic responses and/or suppress proliferation and growth of DNPC in vitro and in vivo.*

### Accomplishments under these goals:

*Aim 1: Identify cell survival and growth-promoting mechanisms that are active in human castration-resistant ‘double negative’ prostate cancers devoid of AR activity*

To achieve the goals of AIM1, I aided in the creation and characterization of DNPC cell lines. These DNPC cell lines were used to identify corroborate findings from RNA-seq analyses of patient tumors. This contributed to a published study<sup>6</sup> (APPENDIX: Androgen Receptor Pathway-Independent Prostate Cancer Is Sustained through FGF Signaling). The major findings of this study include:

- 1) The frequency of double-negative (AR-null; NE-null) prostate cancer is increasing
- 2) FGF and MAPK pathways are active in AR-null prostate cancer
- 3) Autocrine and paracrine FGF pathway activation can bypass AR dependence
- 4) Targeting the FGF and MAPK pathways can repress AR-null prostate cancer..

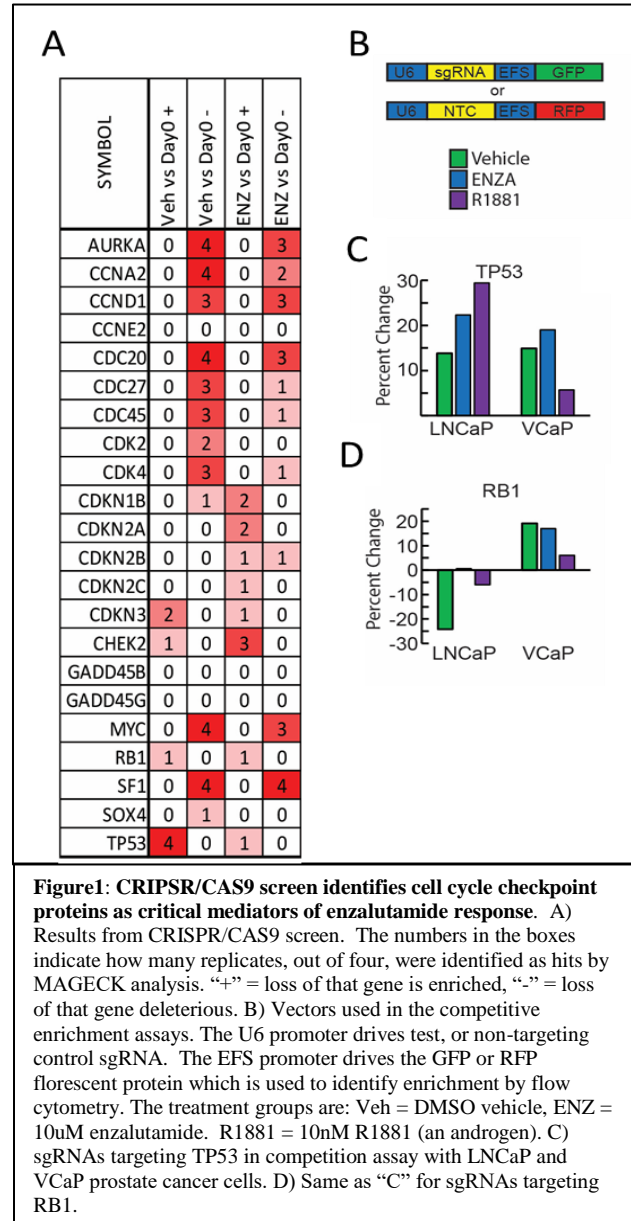
*Aim 2: Utilize genome-wide screening approaches to define signaling pathways capable of sustaining AR-null prostate cancer growth.*

To identify factors that mediate complete independence from AR-activity, we first identified factors that mediated resistance to ENZ. To this end we performed CRISPR/CAS9 screens in the prostate cancer cell line LNCaP. Cells were cultured for 25 days with 10uM ENZ, harvested, barcoded, and sent for high-throughput sequencing to the Fred Hutch Genomic Core. Results were analyzed using the MAGECK analysis platform<sup>7</sup>. A results summary is shown in **Figure1A**. Cell-cycle factors were prominent hits of this screen including MYC, TP53, and RB1.

Since TP53 and RB1 loss are enriched in AR-null prostate cancers<sup>5</sup>. We investigated these factors for their ability to mediate ENZ resistance. To confirm that they mediate ENZ resistance we performed competitive enrichment assays using constructs in **Figure1B**. For the competitive enrichment assays, oligos were clones into a modified version of pLentiCRISPRv2 that contains turboGFP or mCherry in place of the CAS9. The CAS9 was cloned into pLenti6.3/V5-DEST via gateway cloning for these experiments (Thermo, #V53306). Cells were transduced with one or both of the TP53 and RB1 sgRNAs and mixed in equal numbers for the assay. Cells were cultured for 25 days in FBS containing media with either DMSO, 10uM enzalutamide, or 10nM R1881 then analyzed by flow cytometry. We found TP53 loss was strongly enriched under all culture conditions (**Figure1C**) whereas RB1 was only enriched in VCaPs (**Figure1D**). It is possible that RB1 loss requires TP53 loss due to the p53-dependent tumor suppressive effects of E2F1.

To establish isogenic models of TP53 and RB1 loss in a castration sensitive prostate cancer cells we used CRISPR/CAS9 to create single knockouts (SKOs) of TP53 and RB1 in LNCaP cells. We isolated three TP53 and RB1 knockout clones each and validated the genetic status via immunoblot (**Figure2A**). The TP53 and RB1 knockout clones had similar levels of RB1 and TP53, respectively, as the parental cell line (**Figure2A**). Adding the antiandrogen enzalutamide did not affect the protein levels of TP53 or RB1 but both were modestly reduced by 10nM R1881, a synthetic AR agonist (**Figure2A**).

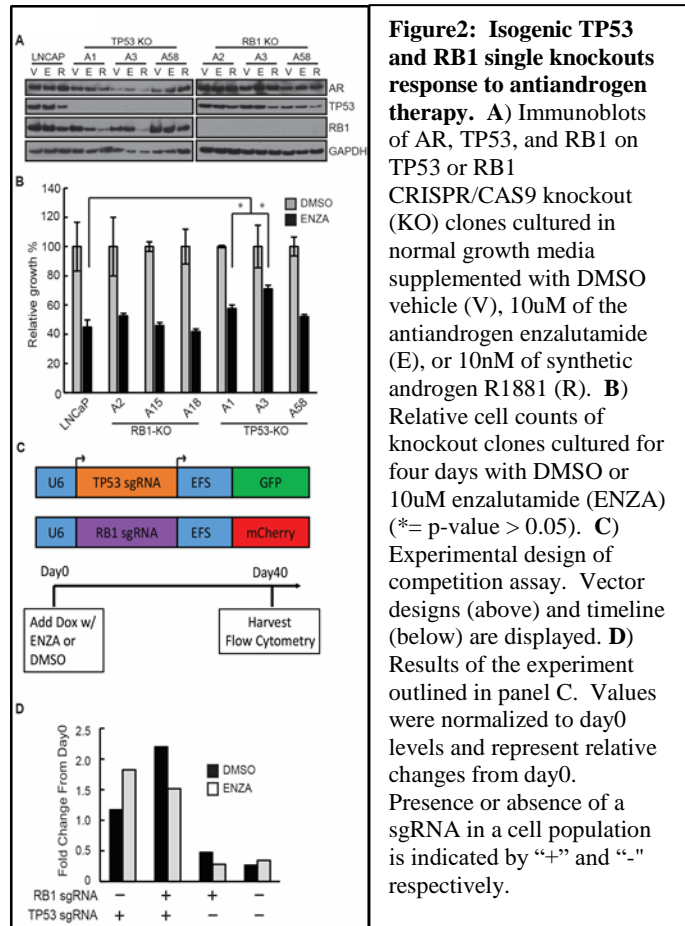
To determine response to antiandrogen of TP53 or RB1 SKOs, we cultured the lines for 96 hours in FBS-containing media with 10uM enzalutamide or vehicle control and counted cell numbers (**Figure2B**). RB1-loss alone did not significantly increase resistance to enzalutamide while two of three TP53-knockout clones were significantly less growth suppressed (**Figure2B**). To evaluate the effect of combined tumor suppressor loss we performed a competitive enrichment assay wherein sgRNAs targeting either TP53 or RB1 are co-expressed with GFP and mCherry respectively (**Figure2C**). Briefly, cells are transduced with one, both, or neither of the



sgRNAs and cultured for 40 days in normal growth media with vehicle or 10uM enzalutamide then analyzed by flow cytometry. Both the single RB1-sgRNA and the no sgRNA groups decreased in frequency relative to the TP53-sgRNA and dual-sgRNA groups under all treatment conditions (**Figure2D**). The single TP53-sgRNA and dual-sgRNA groups were enriched in the vehicle condition whereas the dual-sgRNA group was the most enriched in the enzalutamide condition (**Figure2D**). Consistent with previous findings<sup>8</sup>, these data suggest that TP53 loss mediates modest resistance to ADT. While RB1 loss alone was less effective in mediating resistance to hormone therapy, RB1 loss in the context of TP53 loss strongly increased resistance to ADT.

To establish double TP53 and RB1 knockout (**DKO**) clones, we knocked out TP53 in two RB1-KO clones, A15 and A18 and confirmed genetic loss by immunoblot (**Figure3A**). One clone, B71, had residual protein expression, consistent with three out of four copy loss (LNCaPs are pseudotetraploid). All but one DKO clone, B29 ( $p = 0.07$ ), was more resistant to enzalutamide than parental LNCaPs. However, the growth of all double knockout clones was still suppressed by enzalutamide (**Figure3B**). In parental LNCaPs, enzalutamide arrested cells in the G1-phase of the cell cycle (**Figure3C**). Dual loss of TP53 and RB1 increased occupancy in the S- and G2-phases of the cell cycle in both enzalutamide and vehicle culture conditions (**Figure3C**).

While enzalutamide suppressed the relative growth of DKO cells, their absolute growth was accelerated compared to LNCaP and the SKO cells (**Figure3D**). We also performed colony forming assays in the presence of 10uM enzalutamide or vehicle on LNCaPs and DKO clones A40 and B72. Colony forming assays were performed by plating 800 cells/well in 12-well plates. Cells were grown for 16 days in FBS media with DMSO or 10uM enzalutamide. Cells were fixed with 2% glutaraldehyde in PBS and stained with crystal violet. Cell cycle analysis was performed using Click-iT EdU Alexa Fluor 488 Flow Cytometry Assay Kit (ThermoFisher, #C10420) and FxCycle Violet Stain (ThermoFisher, #F10347).



DKO cells also displayed an accelerated 16-day colony formation under both vehicle and enzalutamide conditions compared to parental LNCaP, the clones of which were not yet visible (**Figure3E**).

Previous studies found that shRNA suppression of TP53 and RB1 resulted in immediate upregulation of SOX2 and gain of plastic or neuroendocrine-like features<sup>5</sup>. To measure changes to cellular plasticity we performed qRT-PCR for prostate epithelial and neuroendocrine markers in LNCaP and DKO-B72 cells exposed to vehicle, 10  $\mu$ M ENZ, or 10 nM R1881 for 48 hours. We also included DKO-B72 cells that have been cultured over 4 months in charcoal-stripped serum (CSS) to mimic the effects of long-term ADT. The AR-regulated genes KLK3 and FKBP5 are expressed in

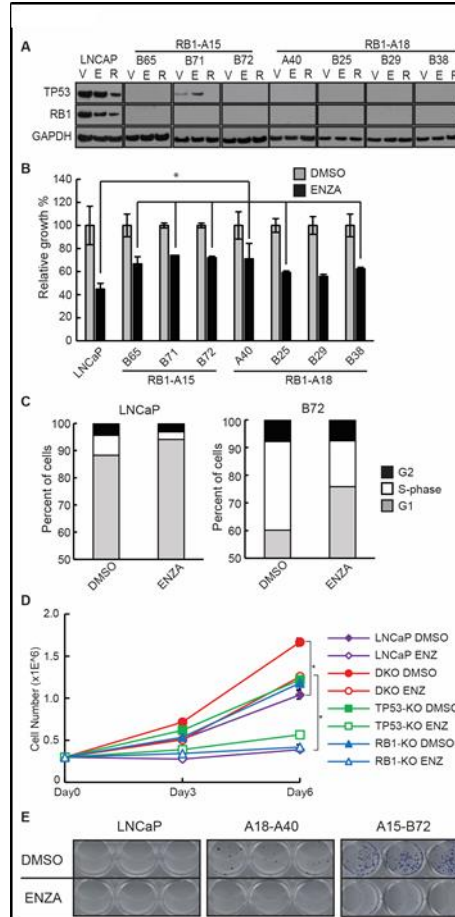


**Figure3: Isogenic TP53 and RB1 double knockouts response to antiandrogen therapy.** **A)** Immunoblots of TP53 and RB1 on double knockout (DKO) clones cultured in normal growth media supplemented with DMSO vehicle (V), 10 $\mu$ M of the antiandrogen enzalutamide (E), or 10nM of synthetic androgen R1881 (R). **B)** Relative cell counts of DKO clones cultured for four days with DMSO or 10 $\mu$ M enzalutamide (ENZA) (\*= p-value > 0.05). **C)** Cell cycle analysis comparing LNCaP and DKO-B72 cells with 10 $\mu$ M enzalutamide (ENZA) or vehicle (DMSO). **D)** Six-day growth assay comparing the absolute growth of LNCaP, DKO-B72, TP53-KO-A58, and RB1-KO-A18. **E)** 16-day colony forming assay of LNCaP and two DKO clones with or without 10 $\mu$ M enzalutamide in normal growth media. (\*= p-value > 0.05)

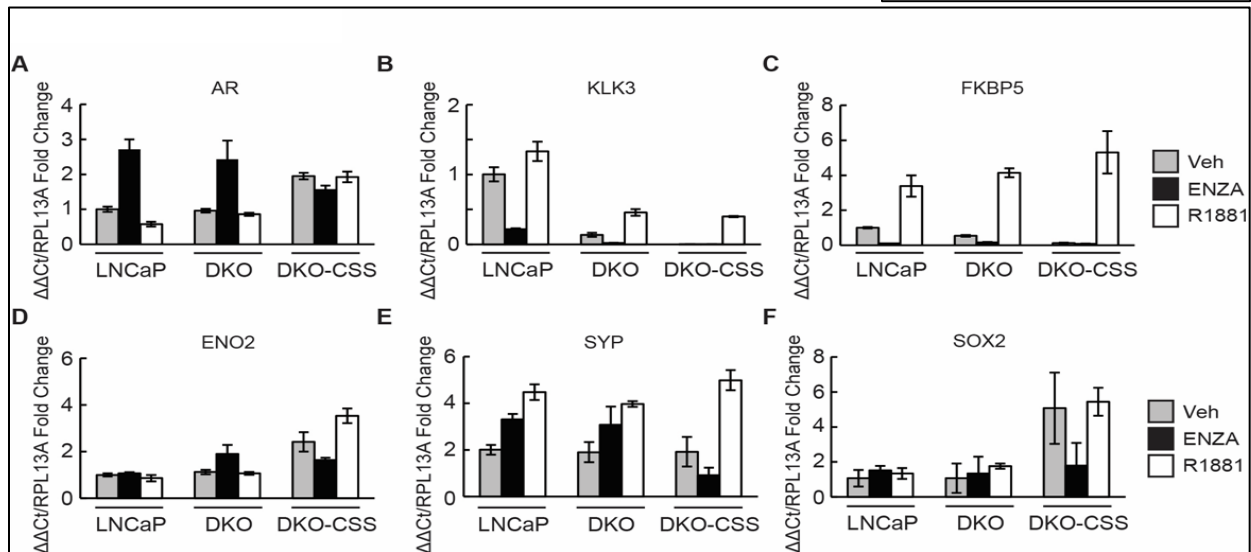


**Figure4: Differentiation genes in dual TP53 and RB1 knockout cells compared to LNCaPs.** qRT-PCR for markers of differentiation on LNCaPs, DKO-B72 cells, and DKO-B72 cells cultured over four months in charcoal-stripped serum (CSS). 10 $\mu$ M enzalutamide, 10nM R1881, and DMSO vehicle were applied to cells for 48 hours. Relative expression of genes associated with prostate adenocarcinoma: **A)** AR; **B)** KLK3(PSA); and **C)** FKBP5. And neuroendocrine or small cell prostate cancer: **D)** ENO2; **E)** SYP; **F)** SOX2.

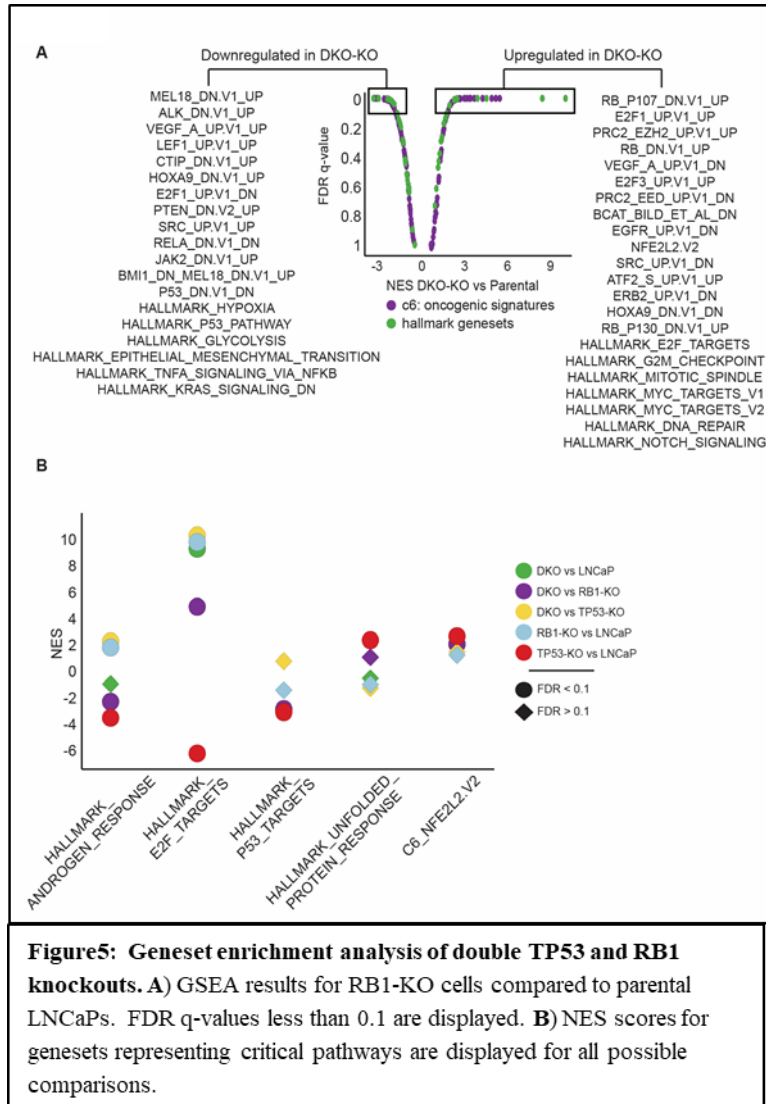
prostate adenocarcinoma where as ENO2, SYP, and SOX2 are highly expressed in neuroendocrine prostate cancer. DKO cells express similar levels of AR as the parental LNCaP (**Figure4A**). KLK3(PSA) expression was reduced in DKO cells but not FKBP5 (**Figure4B,C**). ENO2 was slightly upregulated in DKO cells grown in CSS media but not SYP (**Figure4D,E**). SOX2 was barely detectable by qRT-PCR and wasn't changed in DKO cells but did increase slightly with long term CSS treatment (**Figure4F**).

Geneset enrichment analysis of RNA-seq performed on the DKO cells revealed combined characteristics of TP53 and RB1 knockout; Genesets representing E2F/RB-loss, MYC, and cell-cycle are upregulated whereas TP53 regulated genesets are downregulated (**Figure5A**). We examined the combinatorial effects of TP53 and RB1 loss by comparing transcriptional changes between DKO and SKO lines (**Figure5B**). TP53-loss reduced androgen regulated gene expression in both the TP53-KO vs LNCaP and the DKO vs RB1-KO comparison. RB1 loss upregulated AR target genes in the RB1-KO vs LNCaP and DKO vs TP53KO comparison.

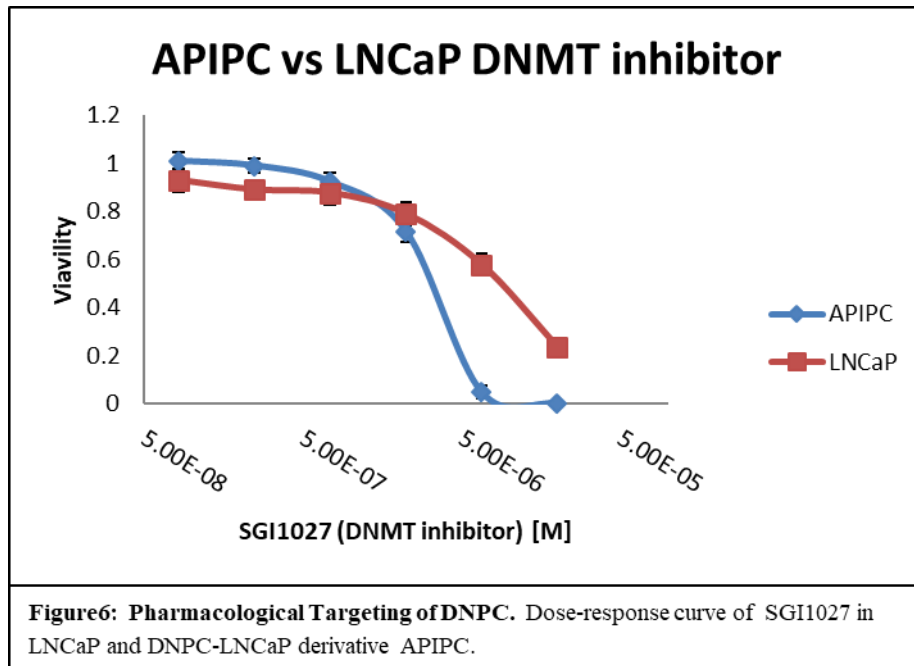
The DKO vs LNCaP showed no significant change. Expectedly, E2F family target genes were upregulated in all RB1 loss clones regardless of TP53 status and p53 targets were downregulated in all TP53-loss clones. The stress response pathway HALLMARK\_UNFOLDED\_PROTEIN\_RESPONSE seen in single TP53 loss clones was not upregulated in the DKO lines. The NFE2L2 (Nrf2) loss geneset was significantly enriched in all TP53-loss comparisons.

From these data, we can conclude that TP53/RB1 loss results in significant loss of differentiation and resistance to antiandrogen. However, DKO cells still retain AR activity and partial dependence on androgen for growth. It is likely that additional factors are likely necessary for the creation of DNPC. Potentially, TP53 and RB1 are necessary for the transition to DNPC but other oncogenic or epigenetic changes are also required for the process.

*Aim 3: Determine whether genetic and pharmacological inhibition of AR-bypass pathways can induce apoptotic responses and/or suppress proliferation and growth of DNPC in vitro and in vivo.*



In our recently published study<sup>6</sup>, we determined that FGF and MAPK inhibitors were had enhanced efficacy against DNPC. (APPENDIX: Androgen Receptor Pathway-Independent Prostate Cancer Is Sustained through FGF Signaling). These targets comprise our top clinical prospects for targeting DNPC. However, in case a DNPC is not sensitive to MAPK/FGFR inhibition, or becomes resistant, we sought to identify additional targets. To find additional inhibitors, we performed a high-throughput drug screen with a ~1400 compound Inhibitor Library (Selleckchem.com). For the screen, LNCaP and AIPIC (an AR-null LNCaP derivative) cells were plated in drug and cultured for 4 days then harvested with CellTiter-Glo (Promega, cat#G7572). One candidate drug hit was validated, de novo methyltransferase inhibitor SGI1027 (Figure6).



We plan to evaluate this drug *in vivo* in naturally occurring DNPC PDX model LuCaP173<sup>6</sup>. If SGI1027 can efficiently suppress the growth of LuCaP173, we will pursue mechanistic studies to determine the mechanism of the sensitivity. Additionally, we are in the process of generating MAPK/FGFR resistant DNPC cell lines. We will target these lines with SGI1027 to determine efficacy.

### Training and professional development provided by project.

During this project I have advanced my understanding to aggressive variants of prostate cancer and AR-bypass pathways through the collaborative effort to understand DNPC and the role of FGFR/MAPK signaling. Specific areas of advancement include regulation of the cell cycle, AR-mediated gene repression, and kinase-driven signaling cascades.

Through my effort to discover the genetic underpinnings of DNPC I learned how to analyze and interpret RNA-seq including becoming proficient in the R and Bash programming and command languages as well as pathway analysis tools and datasets (e.g. GSEA, GSEA, GO, KEGG). Studying the nuances of transcriptional regulation and the complex interactions of transcription factors has furthered my knowledge of AR-biology and pathways that intersect with it.

I also learned how to design, implement, analyze, and validate whole-genome CRISPR screens. And how to design, interpret, and validate high-throughput drug screens. The combination of increased technical proficiency with cutting-edge laboratory techniques and a more developed understanding of AR-biology has enhanced my ability to conduct prostate cancer research.

### Dissemination of results to communities of interest

Currently the only publication that insects with the data generated for this project is our FGF and MAPK in DNPC publication. (APPENDIX: Androgen Receptor Pathway-Independent Prostate Cancer Is Sustained through FGF Signaling.

We are currently preparing a manuscript on the TP53 and RB1 knockout cell lines and plan to submit it for publication within the current year.

Publication of the drug screen and SGI1027 will be contingent on further validation studies into the efficacy of this compound on other DNPC models.

### **Plan for next reporting period**

Nothing to report

### **IMPACT**

#### **Impact on the development of the principal discipline**

Work comprising AIM1 and AIM3 of this project contributed to the publication of an influential study wherein a new subtype of advanced prostate cancer, DNPC, is histologically, genetically, and molecularly defined. We also provide evidence that DNPC is a growing in prevalence with the use of next-generation AR therapies such as enzalutamide and abiraterone. We identified critical pathways that support the growth and survival of DNPC, such as FGF/MAPK, and demonstrate that pharmacologically inhibiting this pathway results in anti-tumor efficacy. Furthermore, the identification of SGI1027 represents another potential avenue to treat an otherwise treatment-refractory DNPC subtype. Future work in the prostate cancer field will now address this growing subtype of cancer and uncover new signaling and genetic mechanism that control the growth of DNPC.

In AIM2 we attempted to define the molecular underpinnings of DNPC. To that end we investigated the potential role of dual TP53 and RB1 loss has on the development of AR-null tumors. It is significant that even with coordinate knockout of both tumor suppressors, which resulted in a rise in proliferation and plasticity, the cancer cells remained AR-responsive. This study sheds light on two critical tumor suppressors in prostate cancer by establishing their phenotype and characterizing their transcriptional consequences. While, further work to uncover how dual loss of these factors can cooperate with other factors to induce DNPC is required. We believe that the signaling changes brought on by the loss of these tumor suppressors is necessary to the transition.

#### **Impact on other disciplines**

From our work, we can envision other hormone dependent cancers, such as breast, to benefit from our insight into the critical role of FGF/MAPK in the transition to hormone independence. Potentially, this pathway is used in other hormone-driven cancers to uncouple the cell from its addiction to receptor signaling.

#### **Impact on technology transfer**

Nothing to report

#### **What was the impact on society beyond science and technology**

Nothing to report

## CHANGES/PROBLEMS:

Nothing to report

## PRODUCTS

### Journal publications

Androgen Receptor Pathway-Independent Prostate Cancer Is Sustained through FGF Signaling. Bluemn EG, Coleman IM, Lucas JM, Coleman RT, Hernandez-Lopez S, Tharakan R, Bianchi-Frias D, Dumpit RF, Kaipainen A, Corella AN, Yang YC, Nyquist MD, Mostaghel E, Hsieh AC, Zhang X, Corey E, Brown LG, Nguyen HM, Pienta K, Ittmann M, Schweizer M, True LD, Wise D, Rennie PS, Vessella RL, Morrissey C, Nelson PS. *Cancer Cell*. 2017 Oct 9;32(4):474-489.e6. doi: 10.1016/j.ccell.2017.09.003.

## PARTICIPANTS & OTHER COLLABORATING ORGANIZATIONS

No change

## SPECIAL REPORTING REQUIREMENTS

Nothing to report

## APPENDICES

### Cited works

1. Berger, M. F. *et al.* The genomic complexity of primary human prostate cancer. *Nature* **470**, 214–20 (2011).
2. Tan, H.-L. *et al.* Rb Loss Is Characteristic of Prostatic Small Cell Neuroendocrine Carcinoma. *Clin. Cancer Res.* **20**, 890–903 (2014).
3. Zhou, Z. *et al.* Synergy of p53 and Rb deficiency in a conditional mouse model for metastatic prostate cancer. *Cancer Res.* **66**, 7889–7898 (2006).
4. Ku, S. Y. *et al.* *Rb1* and *Trp53* cooperate to suppress prostate cancer lineage plasticity, metastasis, and antiandrogen resistance. *Science* (80-. ). **355**, 78–83 (2017).
5. Mu, P. *et al.* SOX2 promotes lineage plasticity and antiandrogen resistance in TP53- and RB1-deficient prostate cancer. *Science* **355**, 84–88 (2017).
6. Bluemn, E. G. *et al.* Androgen Receptor Pathway-Independent Prostate Cancer Is Sustained through FGF Signaling. *Cancer Cell* **32**, 474–489.e6 (2017).
7. Li, W. *et al.* MAGeCK enables robust identification of essential genes from genome-scale CRISPR/Cas9 knockout screens. *Genome Biol.* **15**, 554 (2014).
8. Robinson, D. *et al.* Integrative clinical genomics of advanced prostate cancer. *Cell* **161**, 1215–1228 (2015).

**Androgen Receptor Pathway-Independent Prostate Cancer Is Sustained through FGF Signaling****Highlights**

- The frequency of double-negative (AR-null; NE-null) prostate cancer is increasing
- FGF and MAPK pathways are active in AR-null prostate cancer
- Autocrine and paracrine FGF pathway activation can bypass AR dependence
- Targeting the FGF and MAPK pathways can repress AR-null prostate cancer

**Authors**

Eric G. Bluemn, Ilsa M. Coleman, Jared M. Lucas, ..., Robert L. Vessella, Colm Morrissey, Peter S. Nelson

**Correspondence**

cmorriss@uw.edu (C.M.),  
pnelson@fhcrc.org (P.S.N.)

**In Brief**

Bluemn et al. show that androgen receptor (AR) inhibition results in a phenotypic shift in castration-resistant prostate cancer, leading to tumors that are AR-null but not neuroendocrine (NE). Models for AR-null, non-NE tumors show elevated FGF and MAPK activity and are sensitive to blockade of these pathways.



# Androgen Receptor Pathway-Independent Prostate Cancer Is Sustained through FGF Signaling

Eric G. Bluemn,<sup>1,2,9</sup> Ilsa M. Coleman,<sup>2,9</sup> Jared M. Lucas,<sup>2</sup> Roger T. Coleman,<sup>2</sup> Susana Hernandez-Lopez,<sup>2</sup> Robin Tharakan,<sup>2</sup> Daniella Bianchi-Frias,<sup>2</sup> Ruth F. Dumpit,<sup>2</sup> Arja Kaipainen,<sup>2</sup> Alexandra N. Corella,<sup>2</sup> Yu Chi Yang,<sup>2</sup> Michael D. Nyquist,<sup>2</sup> Elahe Mostaghel,<sup>1,2</sup> Andrew C. Hsieh,<sup>1,2</sup> Xiaotun Zhang,<sup>3</sup> Eva Corey,<sup>3</sup> Lisha G. Brown,<sup>3</sup> Holly M. Nguyen,<sup>3</sup> Kenneth Pienta,<sup>6</sup> Michael Ittmann,<sup>7</sup> Michael Schweizer,<sup>1</sup> Lawrence D. True,<sup>4</sup> David Wise,<sup>5</sup> Paul S. Rennie,<sup>8</sup> Robert L. Vessella,<sup>3</sup> Colm Morrissey,<sup>3,\*</sup> and Peter S. Nelson<sup>1,2,3,4,10,\*</sup>

<sup>1</sup>Department of Medicine, University of Washington, Seattle, WA, USA

<sup>2</sup>Divisions of Human Biology and Clinical Research, Fred Hutchinson Cancer Research Center, Mailstop D4-100, 1100 Fairview Avenue N, Seattle, WA 98109-1024, USA

<sup>3</sup>Department of Urology, University of Washington, 1959 NE Pacific Street, Seattle, WA 98195, USA

<sup>4</sup>Department of Pathology, University of Washington, Seattle, WA, USA

<sup>5</sup>Memorial Sloan-Kettering Cancer Center, New York, NY, USA

<sup>6</sup>Johns Hopkins University, Baltimore, MD, USA

<sup>7</sup>Baylor College of Medicine, Houston, TX, USA

<sup>8</sup>Vancouver Prostate Centre, Vancouver, BC, Canada

<sup>9</sup>These authors contributed equally

<sup>10</sup>Lead Contact

\*Correspondence: [cmorris@uw.edu](mailto:cmorris@uw.edu) (C.M.), [pnelson@fhcrc.org](mailto:pnelson@fhcrc.org) (P.S.N.)

<http://dx.doi.org/10.1016/j.ccell.2017.09.003>

## SUMMARY

Androgen receptor (AR) signaling is a distinctive feature of prostate carcinoma (PC) and represents the major therapeutic target for treating metastatic prostate cancer (mPC). Though highly effective, AR antagonism can produce tumors that bypass a functional requirement for AR, often through neuroendocrine (NE) transdifferentiation. Through the molecular assessment of mPCs over two decades, we find a phenotypic shift has occurred in mPC with the emergence of an AR-null NE-null phenotype. These “double-negative” PCs are notable for elevated FGF and MAPK pathway activity, which can bypass AR dependence. Pharmacological inhibitors of MAPK or FGFR repressed the growth of double-negative PCs *in vitro* and *in vivo*. Our results indicate that FGF/MAPK blockade may be particularly efficacious against mPCs with an AR-null phenotype.

## INTRODUCTION

Androgen deprivation therapy (ADT), achieved through surgical or pharmacological approaches, exploits the exquisite dependence of prostate carcinoma (PC) on androgen receptor (AR) signaling. Although initially highly effective as a treatment for metastatic PC, ADT is characterized by the predictable emergence of resistance, a disease state termed castration-resistant prostate cancer (CRPC). An important feature of CRPC is the reactivation of AR signaling, an event reflected by progressive rises in serum prostate-specific antigen (PSA), a gene product tran-

scriptionally regulated by the AR. A substantial body of evidence has documented that essentially the entire AR cistrome is re-expressed in most CRPCs, and several mechanisms capable of maintaining AR activity have been established (Carver *et al.*, 2011; Montgomery *et al.*, 2008; Nelson *et al.*, 2002; Taylor *et al.*, 2010).

The continued importance of AR signaling in most advanced PCs has prompted the development of therapeutics directed toward further suppressing AR ligands or the AR itself. Several drugs, including improved AR antagonists and inhibitors of androgen synthesis, extend survival (de Bono *et al.*, 2011; Scher

### Significance

Targeting AR signaling in metastatic PC commonly produces robust clinical responses. However, disease progression is nearly universal. Potent AR antagonists appear to be shifting the phenotypes of resistant PCs to tumors that are devoid of AR activity, but the drivers of these resistant carcinomas are not known. Here we report that autocrine and paracrine FGF signaling is capable of bypassing a requirement for AR, and find that FGF and MAPK pathways are active in metastatic AR-null PCs. Suppressing FGF and MAPK inhibits the growth of AR-null PC indicating that targeting the FGF axis may represent a therapeutic approach for those cancers resistant to AR-directed therapies and may circumvent treatment resistance if combined with initial AR pathway blockade.

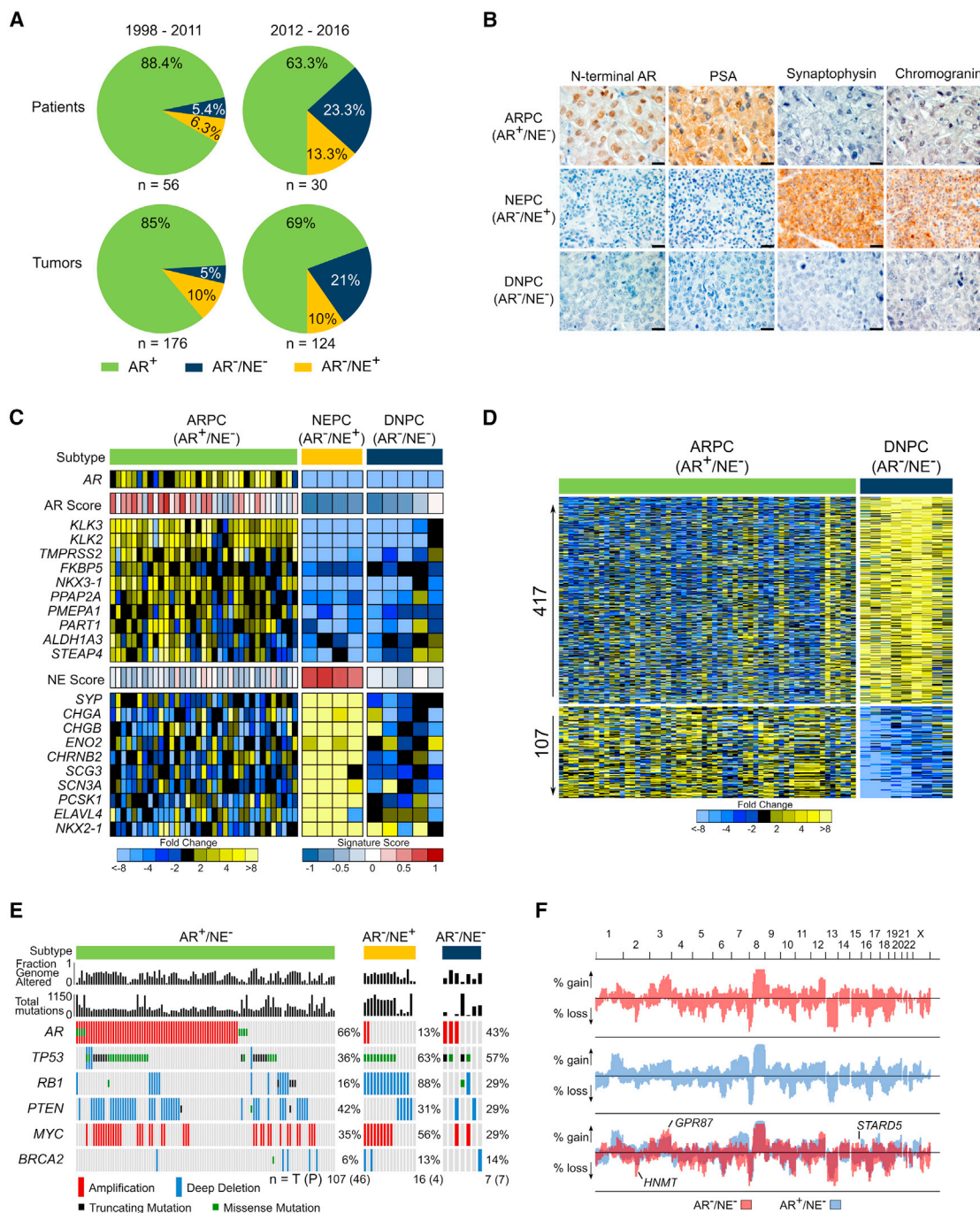


### Figure 1. Molecular Features of AR-Null Neuroendocrine-Null Prostate Cancer

(A) The frequency of AR-active prostate cancers (ARPC), neuroendocrine prostate cancers (NEPC), and double-negative AR-null/neuroendocrine-null prostate cancers (DNPC) in men with metastatic CRPC evaluated in consecutive tissue acquisition necropsies from 1998 to 2016. Numbers of tumors and patients in each cohort is shown.

(B) Representative immunohistochemical stains for AR, PSA, synaptophysin and chromogranin used to classify metastases as ARPC, NEPC, or DNPC. Scale bars, 20  $\mu$ m.

(C) RNA sequencing-based measurements of transcripts comprising AR-regulated genes and neuroendocrine phenotype-associated genes in metastatic tumors from men with CRPC. Signature scores are shown above each gene set. Expression profile of one representative tumor per patient is shown, (AR<sup>+</sup>/NE<sup>-</sup>, n = 35; AR<sup>-</sup>/NE<sup>+</sup>, n = 4; AR<sup>-</sup>/NE<sup>-</sup>, n = 5.)

(D) Differentially expressed genes in ARPC compared with DNPC (5-fold difference; q value <0.0001). Transcript abundance was determined by RNA sequencing and analyzed for differential expression using the Bioconductor edgeR software (ARPC, n = 58 tumors from 35 men; DNPC, n = 9 tumors from 5 men).

(legend continued on next page)

et al., 2012), although to date complete remissions have been rare. While the intensive effort focused on completely repressing AR activity may completely eradicate a subset of PCs, this selective pressure has the potential to generate PCs reliant on survival mechanisms distinct from those regulated by AR or that substitute for vital AR functions.

Assessments of metastatic CRPCs have determined that patients may harbor tumor deposits that do not express AR following conventional ADT (Roudier et al., 2003; Shah et al., 2004). While a subset of AR-null tumors express markers of neuroendocrine (NE) differentiation, these neuroendocrine prostate cancers (NEPC) exist within a more complex spectrum of phenotypes ranging from anaplastic carcinomas, mixed prostatic adenocarcinomas with NE features, to pure small-cell carcinomas (Aparicio et al., 2011; Beltran et al., 2011; Tzelepi et al., 2012). Importantly, there are metastatic CRPCs that do not express the AR or markers of NE differentiation (Roudier et al., 2003; Wang and Epstein, 2008). Although conclusive data are lacking, evidence suggests that the widespread application of more effective AR pathway antagonists such as enzalutamide (ENZ) and abiraterone (ABI) is shifting the pattern of metastasis in patients with CRPC accompanied by alterations in their molecular landscapes (Beltran et al., 2014; Doctor et al., 2014). Anticipating that effective AR repression will more routinely result in CRPCs devoid of AR signaling, we sought to identify molecular pathways operating in CRPC that function to promote survival and growth in the absence of AR activity. The emergent signaling programs that confer resistance to AR-directed therapeutics may represent treatment targets for men with progressive CRPC.

## RESULTS

### Emergence of an AR-Null and Neuroendocrine-Null Prostate Cancer Phenotype in Patients Following AR-Directed Therapy

To evaluate the shifting phenotypic and molecular landscapes of metastatic CRPC (mCRPC), we characterized metastatic tumors acquired from a long-standing tissue acquisition necropsy program spanning two decades. We classified tumors from 84 consecutive patients as androgen receptor pathway active prostate cancer (ARPC) if they expressed AR and the AR-regulated gene PSA, or NEPC if they expressed the NE gene synaptophysin (SYP). In a small minority of patients both ARPC and NEPC tumors were evident. In the era prior to the approval of the AR pathway antagonists ENZ and ABI (1997–2011), most CRPCs were ARPCs (85%) with rare NEPCs (10%) and rarer AR<sup>-</sup>/NE<sup>-</sup> tumors (5%), hereafter classified as “double-negative” PCs (DNPC) (Figures 1A and 1B). In the contemporary era (2012–2016), we observed a shift in tumor phenotypes with a higher representation of DNPCs (Figure 1A). Gene expression programs

of the tumors classified by immunohistochemistry (IHC) supported these distinct subtypes using 10-gene signatures that were concordant with previously published gene sets indicative of NE and AR pathway activity (Figures 1C, S1A, and S1B) (Beltran et al., 2016; Hieronymus et al., 2006).

While molecular characteristics of CRPCs with active AR and NE programs are well described, those of DNPC are not established. We used RNA sequencing (RNA-seq) to quantitate gene expression differences between DNPCs and ARPCs and identified 417 and 107 mRNAs with substantially increased or decreased levels, respectively (5-fold;  $q < 0.0001$ ) (Figure 1D). In comparison with NEPC, 162 and 594 genes were significantly increased or decreased, respectively in DNPCs (5-fold;  $q < 0.0001$ ) (Figure S1C). Gene set enrichment analysis (GSEA) identified numerous biological processes that differed between ARPC and DNPC, which complicated efforts to identify a predominant driver event or signaling pathway (Figure S1D). To prioritize efforts defining causal mechanisms underlying DNPC, we evaluated tumors for genomic alterations and partitioned mCRPCs that we previously characterized for genome-wide copy-number and mutation status (Kumar et al., 2016) into categories of ARPC, NEPC, and DNPC based on their expression profiles (Figures 1E, 1F, S1E, and S1F). Common aberrations in CRPCs such as *TP53* mutation and *PTEN* loss did not differ significantly across groups with the exception of *AR* amplification, which was more frequent in ARPC (66%) compared with NEPC (13%) ( $p = 5.6 \times 10^{-5}$ ) and *RB1* loss, a hallmark of NEPC, which differed between NEPC (88%) and ARPC (16%) ( $p = 2.4 \times 10^{-8}$ ) (Figure 1E). Several genomic regions differed in copy number between ARPC and DNPC, but no genes in these regions varied in expression by more than 2-fold (Figure 1F). With the caveat of limited tumor numbers, these data indicate that recurrent genomic aberrations do not underlie the marked phenotypic differences between ARPC and DNPC.

### AR Ablation Results in CRPC without Neuroendocrine Differentiation

To provide insights into causal mechanisms capable of promoting survival in an AR-null state, we developed a model system that recapitulated the transition from a tumor initially dependent on AR activity to one capable of AR-independent growth. We began with the LNCaP cell line, a widely studied androgen-sensitive *in vitro* model of PC. LNCaP derivatives capable of proliferating in the absence of AR ligands typically continue to exhibit AR signaling (Sobel and Sadar, 2005). Furthermore, targeting the AR in these cells with antibodies, ribozymes, or RNAi induces apoptosis or growth arrest, indicating that the AR maintains vital functions (Cheng et al., 2006; Zegarra-Moro et al., 2002). To initiate the present studies, we used a LNCaP line stably transduced with a tetracycline (TET)-inducible anti-AR short hairpin RNA (shRNA) (Cheng et al., 2006), designated as LNCaP<sup>shAR</sup>.

(E) The frequency of recurrent genomic aberrations in the CRPC subtypes of AR<sup>+</sup>/NE<sup>-</sup> (ARPC), AR<sup>-</sup>/NE<sup>+</sup> (NEPC), and AR<sup>-</sup>/NE<sup>-</sup> (DNPC) determined by aCGH and exome sequencing. Status of individual tumors and percentage altered in each group is shown, with numbers of patients (P) and tumors (T) below the plot.

(F) Frequency of copy-number alterations (CNAs) determined by genome-wide array CGH. Copy-number gains and losses in ARPC (blue), DNPC (red), and shared (purple). Three genes (*HNMT*, *GPR87*, and *STARD5*) were significant by two-tailed Fisher's exact tests comparing the proportion of high copy gains or homozygous losses between the groups ( $p < 0.05$ ) and also exhibited concordant differential mRNA expression by two-sample t test ( $p < 0.05$ ). (DNPC,  $n = 8$  tumors from 8 individuals; ARPC,  $n = 118$  tumors from 52 individuals).

See also Figure S1.

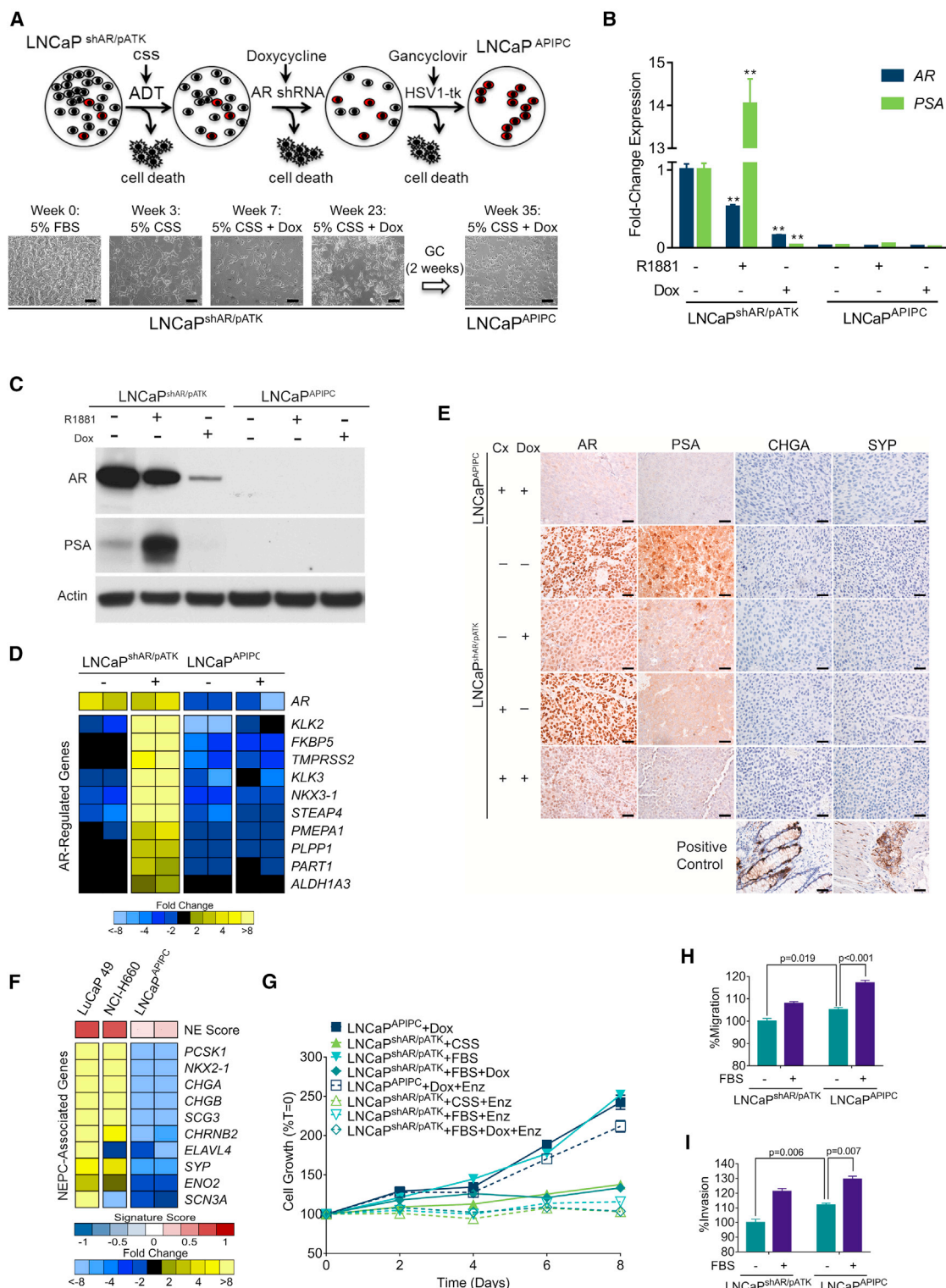


**Figure 2. Characterization of a Model of AR Program-Independent Prostate Cancer**

(A) LNCaP cells with a doxycycline (Dox)-inducible shRNA targeting the AR (shAR) and an androgen-driven thymidine kinase gene (pATK) were starved of androgens (ADT) and treated with Dox to induce the AR-directed shRNA, then treated with gancyclovir to eliminate cells with AR-driven thymidine kinase expression. Scale bars, 10  $\mu$ m.

(B) qRT-PCR analysis of AR and PSA expression in LNCaP<sup>shAR/pATK</sup> and LNCaP<sup>APIPC</sup> with 1 nM R1881 or 1  $\mu$ g/mL Dox treatment. Significance was determined by Student's t test and data are presented as mean  $\pm$  SEM (n = 4 replicates per data point); \*\*p < 0.01.

(legend continued on next page)

Repressing AR in the setting of castration-resistant LNCaP<sup>shAR</sup> growth results in tumor regression, but recurrent LNCaP<sup>shAR</sup> tumors re-express AR, due to the selective loss or silencing of the AR-directed shRNA (Snoek et al., 2009). To enforce AR ablation, we introduced an androgen response element (ARE)-driven thymidine kinase suicide gene designated pATK. In the resulting LNCaP<sup>shAR/pATK</sup> line, thymidine kinase is expressed in the setting of an active AR and induces cell death when treated with ganciclovir (Figures 2A and S2A–S2C).

We subjected LNCaP<sup>shAR/pATK</sup> cells to increasingly severe AR pathway suppression (Figure 2A). After 2 weeks of androgen deprivation (ADT), medium was supplemented with 1  $\mu$ g/mL doxycycline (Dox) to induce the anti-AR shRNA, which produced >99% cell death. After 5 months, a residual population of viable cells remained. This colony was treated with a 2-week course of ganciclovir to eliminate cells expressing functional AR. Surviving cells were designated LNCaP-AR Program-Independent Prostate Cancer (LNCaP<sup>APIPC</sup>). AR and PSA were nearly undetectable in LNCaP<sup>APIPC</sup>; AR expression was 45-fold lower and PSA expression was 30-fold lower than LNCaP<sup>shAR/pATK</sup> (Figures 2B and 2C). Transcripts comprising an AR activity signature were all substantially decreased in LNCaP<sup>APIPC</sup> cells and showed no induction with androgen treatment (Figure 2D). We confirmed the absence of AR and PSA protein expression in LNCaP<sup>APIPC</sup> grown *in vivo* as subcutaneous xenografts (Figure 2E).

Previous studies demonstrated that LNCaP cells grown in androgen-depleted medium or with AR antagonists display a transdifferentiated phenotype resembling NEPC (Mu et al., 2017; Zhang et al., 2003). NEPC is characterized by loss of AR expression and AR activity and increased expression of CHGA and SYP, and cells often exhibit small-cell morphology (Beltran et al., 2011). NE-associated genes were not upregulated in LNCaP<sup>APIPC</sup> cells grown with or without androgen supplementation (Figure 2F). Furthermore, LNCaP<sup>shAR/pATK</sup> and LNCaP<sup>APIPC</sup> grown as murine xenografts do not express CHGA or SYP protein (Figure 2E).

To further evaluate the characteristics of LNCaP<sup>APIPC</sup> cells, we determined the effects of AR pathway-targeted therapies. In contrast to parental LNCaP<sup>shAR/pATK</sup>, LNCaP<sup>APIPC</sup> grow robustly without androgen (Figure 2G). Furthermore, treatment of LNCaP<sup>shAR/pATK</sup> with ENZ completely inhibited growth, while LNCaP<sup>APIPC</sup> was highly resistant to ENZ treatment (Figure 2G). PC cells with low AR transcriptional activity that accompanies advanced Gleason grade exhibit invasive and metastatic phenotypes (Aihara et al., 1994; Erbersdobler et al., 2009). LNCaP<sup>APIPC</sup>

cells displayed a slight but consistent increase in baseline migration (5%,  $p = 0.019$ ) and invasion (12%,  $p = 0.006$ ) when compared with LNCaP<sup>shAR/pATK</sup>, and also responded to a transwell serum gradient with a higher number of migratory and invasive cells (Figures 2H and 2I).

### FGFR and MAPK Signaling Pathways Are Activated in Androgen Receptor Pathway-Independent Prostate Cancer

The growth of LNCaP<sup>APIPC</sup> cells in the absence of AR expression indicated that alternative survival pathways supplanted AR requirements and we next sought to identify them. We used RNA-seq to profile the gene expression program in LNCaP<sup>APIPC</sup> and identified 548 differentially expressed transcripts relative to AR-intact LNCaP<sup>shAR/pATK</sup> cells ( $\geq 10$ -fold;  $q < 0.001$ ) (Figure 3A). LNCaP<sup>APIPC</sup> gained expression of basal cell genes such as *TP63* and *TRIM29*, and retained expression genes expressed in luminal cells such as *KRT8*, *KRT18*, and *HPN* (Figure 3B). We used array CGH to identify copy-number aberrations harboring genes that could bypass a requirement for AR signaling. Overall, the genomes of LNCaP<sup>APIPC</sup> and parental LNCaP<sup>shAR/pATK</sup> were nearly identical, with only seven regions differing in copy number between the two lines. Two genes, *MAT2B* and *KIAA1328*, exhibited concordant changes in copy number and expression, but transcript levels did not differ between ARPCs and DNPCs. Though located in the region of chromosome-3 copy gain, *WNT7A* transcripts were not measurable in LNCaP<sup>APIPC</sup> cells (Figures S3A–S3C). Collectively, the few genomic aberrations identified do not explain the marked alterations in gene expression between LNCaP<sup>APIPC</sup> and parental LNCaP<sup>shAR/pATK</sup> cells.

To confirm lineage relationships, we compared the expression profiles of 15 PC cell lines with LNCaP<sup>APIPC</sup> using unsupervised hierarchical clustering. LNCaP<sup>APIPC</sup> grouped with other LNCaP derivatives, indicating that LNCaP<sup>APIPC</sup> retains LNCaP characteristics even while lacking AR-regulated gene expression (Figure 3C). Notably, the removal of Dox from the culture medium of LNCaP<sup>APIPC</sup> cells did not result in AR re-expression or a reversal of gene expression changes (Figure S4A). We also found no evidence of upregulation of the glucocorticoid receptor (*GR/NR3C1*), a nuclear hormone receptor previously shown to bypass AR requirements (Arora et al., 2013) (Figure 3D).

Phosphatidylinositol 3-kinase (PI3K)/AKT signaling can influence the progression of CRPC and effectively compensate for reduced AR activity in PC models via reciprocal feedback

(C) AR and PSA immunoblots of cell lysates from LNCaP<sup>shAR/pATK</sup> and LNCaP<sup>APIPC</sup> cultured in androgen-depleted conditions and treated with or without R1881 and with or without Dox.

(D) Quantitation of AR-regulated transcripts following treatment with the synthetic androgen R1881 (+) in parental LNCaP<sup>shAR/pATK</sup> and LNCaP<sup>APIPC</sup> cells. Measurements were made by RNA sequencing ( $n = 2$  biological replicates per group).

(E) Immunohistochemical analysis of AR, PSA, CHGA, and SYP in parental LNCaP<sup>shAR/pATK</sup> and LNCaP<sup>APIPC</sup> xenografts. Cx, castration; Dox, doxycycline. Scale bars, 10  $\mu$ m.

(F) Expression of neuroendocrine-associated transcripts in the NEPC LuCaP49 PDX model, NEPC NCI-H660 cell line, and LNCaP<sup>APIPC</sup> cells. Measurements were made by RNA sequencing (RNA-seq) ( $n = 2$  biological replicates of LNCaP<sup>APIPC</sup> cells, 1 each of LuCaP49 and NCI-H660).

(G) LNCaP<sup>APIPC</sup> grown in androgen- and AR-depleted conditions were treated with vehicle (DMSO) or 5  $\mu$ M enzalutamide (ENZ). Growth was compared with parental LNCaP<sup>shAR/pATK</sup> cells in charcoal stripped serum (CSS), fetal bovine serum (FBS), or FBS + 1  $\mu$ g/mL Dox  $\pm$  ENZ. Solid lines, with DMSO vehicle; dotted lines, with ENZ. All values are normalized to day 0. Data are presented as mean  $\pm$  SEM ( $n = 5$  per data point).

(H and I) Transwell migration (H) and invasion assays (I) of LNCaP<sup>shAR/pATK</sup> and LNCaP<sup>APIPC</sup> at baseline (no FBS gradient) and in response to a serum (FBS) gradient. Significance was determined using Student's *t* test and data are presented as mean  $\pm$  SEM ( $n = 4$ ).

See also Figure S2.

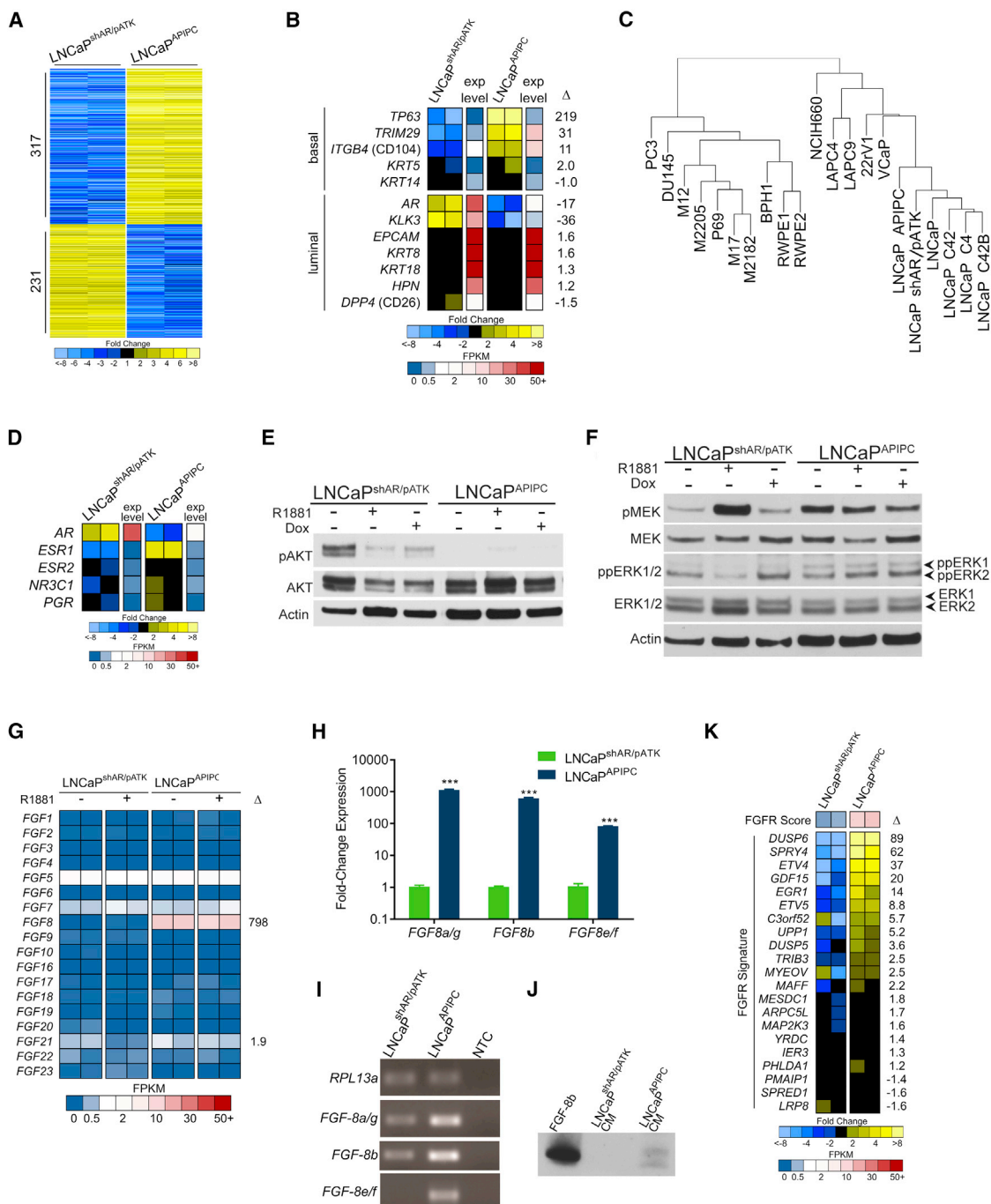


### Figure 3. Assessments of AKT, MAPK, and FGF Pathway Activity in the LNCaP<sup>APIPC</sup> Model of DNPC

(A) Genome-wide assessment of transcripts differentially expressed between LNCaP<sup>shAR/pATK</sup> and LNCaP<sup>APIPC</sup> cells as measured by RNA-seq. Shown are 548 genes with  $q$  values of  $<0.001$  and fold changes of  $\geq 10$  ( $n = 2$  biological replicates per group).

(B) Measurements of luminal and basal cell gene expression in LNCaP<sup>APIPC</sup> cells. Relative ratios of RNA-seq transcript abundances are shown, along with mean FPKM (fragments per kilobase of transcript per million mapped reads) values ( $n = 2$  biological replicates per group).

(C) Unsupervised cluster analysis of gene expression profiles across prostate cancer cell lines associates LNCaP<sup>APIPC</sup> cells with LNCaP cells and sublines. One replicate of each cell line used to cluster RNA-seq profiles of the top 1,000 most variable genes.

(D) Expression of nuclear hormone receptors determined by RNA-seq of LNCaP<sup>shAR/pATK</sup> and LNCaP<sup>APIPC</sup> cells. Relative ratios of RNA-seq transcript abundances are shown, along with mean FPKM values. Two independent biological replicates were sequenced.

(E) PI3K pathway signaling was assessed by probing LNCaP<sup>APIPC</sup> and LNCaP<sup>shAR/pATK</sup> cell lysates with antibodies to AKT and phosphorylated AKT.

(F) MAPK pathway signaling was assessed by probing LNCaP<sup>APIPC</sup> and LNCaP<sup>shAR/pATK</sup> cell lysates with antibodies to MEK, phosphorylated MEK, ERK1/2, and dually phosphorylated ERK1/2.

(legend continued on next page)

activation (Carver et al., 2011; Mulholland et al., 2011). Therefore, we hypothesized that PI3K pathway upregulation was supporting LNCaP<sup>APIPC</sup> growth. Consistent with previous studies, pAKT levels increased in AR-intact LNCaP<sup>shAR/pATK</sup> cells grown in androgen-depleted medium (Figure 3E). Surprisingly, pAKT was nearly undetectable in LNCaP<sup>APIPC</sup>, suggesting that PI3K activity is not acting as a survival/growth pathway in these AR-null cells.

Increased mitogen-activated protein kinase (MAPK) signaling is also postulated to support CRPC proliferation (Aytes et al., 2013; Mulholland et al., 2012; Ueda et al., 2002). MAPK signal transduction is activated through a variety of stimuli, and is closely associated with receptor tyrosine kinase (RTK) activity. Phosphorylated MEK and dually phosphorylated ERK1/2 (ppERK1/2) were elevated in LNCaP<sup>APIPC</sup> compared with LNCaP<sup>shAR/pATK</sup> (Figure 3F). These data suggested that increased MAPK signaling may be sustaining AR-independent growth in LNCaP<sup>APIPC</sup>. We evaluated RAS and RAF for alterations that could account for MAPK activation but found no evidence of altered expression or functional mutations (Figures S4B and S4C).

We next evaluated the LNCaP<sup>APIPC</sup> transcriptome for mechanisms plausibly contributing to MAPK activity and found that *fibroblast growth factor 8* (*FGF8*) expression was substantially upregulated relative to AR-active LNCaP<sup>shAR/pATK</sup> (>100-fold,  $q < 0.001$ ) (Figure 3G). *FGF8* is transcribed as eight distinct isoforms (FGF8a–h), and of these FGF8b has the most oncogenic effects (MacArthur et al., 1995). LNCaP<sup>APIPC</sup> expressed all active FGF8 isoforms at substantially higher levels than LNCaP<sup>shAR/pATK</sup> (FGF8a/g = 1,100-fold,  $p < 0.001$ ; FGF8b = 600-fold,  $p < 0.001$ ) (Figures 3H and 3I). FGF8 protein was detected in serum-free conditioned medium from LNCaP<sup>APIPC</sup> but not from LNCaP<sup>shAR/pATK</sup>, concordant with transcript expression results (Figures 3J and S4D).

To further assess FGF pathway activity, we measured a panel of transcripts shown to reflect the dynamic output of FGF receptor (FGFR) signaling (Delpuech et al., 2016). Several transcripts comprising this FGFR signature were increased more than 10-fold in LNCaP<sup>APIPC</sup> cells including *DUSP6*, *ETV4*, and *EGR1*, and LNCaP<sup>APIPC</sup> cells showed significant FGFR and MAPK pathway enrichment scores (Figure 3K). FGF pathway activation has been shown to occur in rare instances by FGFR genomic rearrangements in mCRPC (Wu et al., 2013), but we found no evidence of mutation, copy-number gain, or gene rearrangements involving *FGF8* or FGFRs in LNCaP<sup>APIPC</sup> (Figures S3B and S3C). Collectively, these data supported the hypothesis that an autocrine FGF signaling program is activated in LNCaP<sup>APIPC</sup> in the absence of AR to maintain cell survival and growth via MAPK.

### FGFR and MAPK Signaling Are Active in DNPC and Are Inversely Associated with AR Activity

We next sought to further evaluate FGF and MAPK signaling in DNPCs and confirm LNCaP<sup>APIPC</sup> as a relevant model for this CRPC subtype. We determined that an LNCaP<sup>APIPC</sup> gene signature is significantly enriched in DNPC metastases (false discovery rate [FDR] < 0.001) (Figure 4A), as are gene sets reflecting the activity of FGF signaling, MAPK activity, MEK/ERK, and EMT (Figure 4B). No single FGF ligand or receptor was universally increased across all DNPCs: individual tumors expressed high *FGF1*, *FGF8*, or *FGF9*, and different FGFRs. Each of these secreted FGF ligands has been shown to activate multiple FGFRs consistent with the finding that DNPCs exhibited consistently high MEK/ERK and FGF activity scores (Figures 4C and 4D). A small subset of ARPCs also expressed high MEK/ERK and FGFR pathway activity, and these tumors generally also had lower AR activity (Figure 4C). Across the full spectrum of CRPC metastases, AR activity was inversely associated with FGF8/9 expression, and FGFR activity (e.g.,  $r = -0.48$ ,  $p < 0.001$  for FGF8) (Figure 4E). AR and FGF8/9 expression were inversely associated ( $r = -0.13$ ) in an independent dataset of 150 metastatic CRPC tumors from the SU2C/PCF dataset (data not shown) (Robinson et al., 2015). Collectively, these results couple elevated FGF and MAPK signaling with a CRPC tumor phenotype, DNPC, which lacks AR activity and supports LNCaP<sup>APIPC</sup> as a model that represents these attributes of DNPC.

To address the challenge of deriving a generalized understanding of DNPC from a single model, we sought to develop additional systems with which to evaluate drivers of DNPC and identify effective therapeutics. As with LNCaP<sup>APIPC</sup>, our objective was to begin with an AR-positive PC and then repress AR activity. We were unable to successfully eliminate AR in the commonly used VCaP or 22Rv1 PC lines by shRNA or CRISPR-based approaches (data not shown). However, using the PacMet-UT1 PC line that expresses a functional AR (Troyer et al., 2008), albeit with attenuated activity, we were able to excise AR using CRISPR/Cas9 editing and generate multiple PacMet AR-null sublines (Figures 5A and 5B). AR loss was associated with 10-fold upregulation of *FGF9* and enhancement of FGF and MAPK activity (Figures 5C and 5D). Notably, repressing AR activity in PacMet-UT1 cells did not result in an NEPC phenotype, and the expression of *SOX2*, a reprogramming factor associated with transdifferentiation to NEPC, was decreased (Figure 5C) (Mu et al., 2017).

We were also successful in generating a patient-derived xenograft (PDX) model of DNPC, designated LuCaP173.2, initiated from a tumor acquired from a rapid autopsy procedure. Metastatic tumors from this individual had phenotypic variability,

(G) Levels of transcripts encoding FGFs were assessed in LNCaP<sup>shAR/pATK</sup> and LNCaP<sup>APIPC</sup> cells by RNA-seq with or without R1881 androgen treatment. Two replicates of each line and treatment were measured, and fold difference between LNCaP<sup>shAR/pATK</sup> and LNCaP<sup>APIPC</sup> cells is shown for FGF8 and FGF21.

(H) Transcript levels of FGF8 mRNAs were measured by qRT-PCR in LNCaP<sup>shAR/pATK</sup> and LNCaP<sup>APIPC</sup>. Significance was determined by Student's *t* test and data are presented as mean  $\pm$  SEM ( $n = 3$  replicates per data point). \*\*\* $p < 0.00001$ .

(I) qRT-PCR reaction products, visualized by agarose gel electrophoresis, confirms single-band amplification by each isoform-specific primer pair.

(J) Assessment of FGF8b protein in conditioned medium (CM) from LNCaP<sup>shAR/pATK</sup> and LNCaP<sup>APIPC</sup> by immunoblotting with an FGF8b-specific antibody.

(K) Expression of genes associated with FGFR pathway activity measured by RNA-seq of LNCaP<sup>shAR/pATK</sup> and LNCaP<sup>APIPC</sup> cells. Two independent biological replicates were sequenced.

See also Figures S3 and S4.

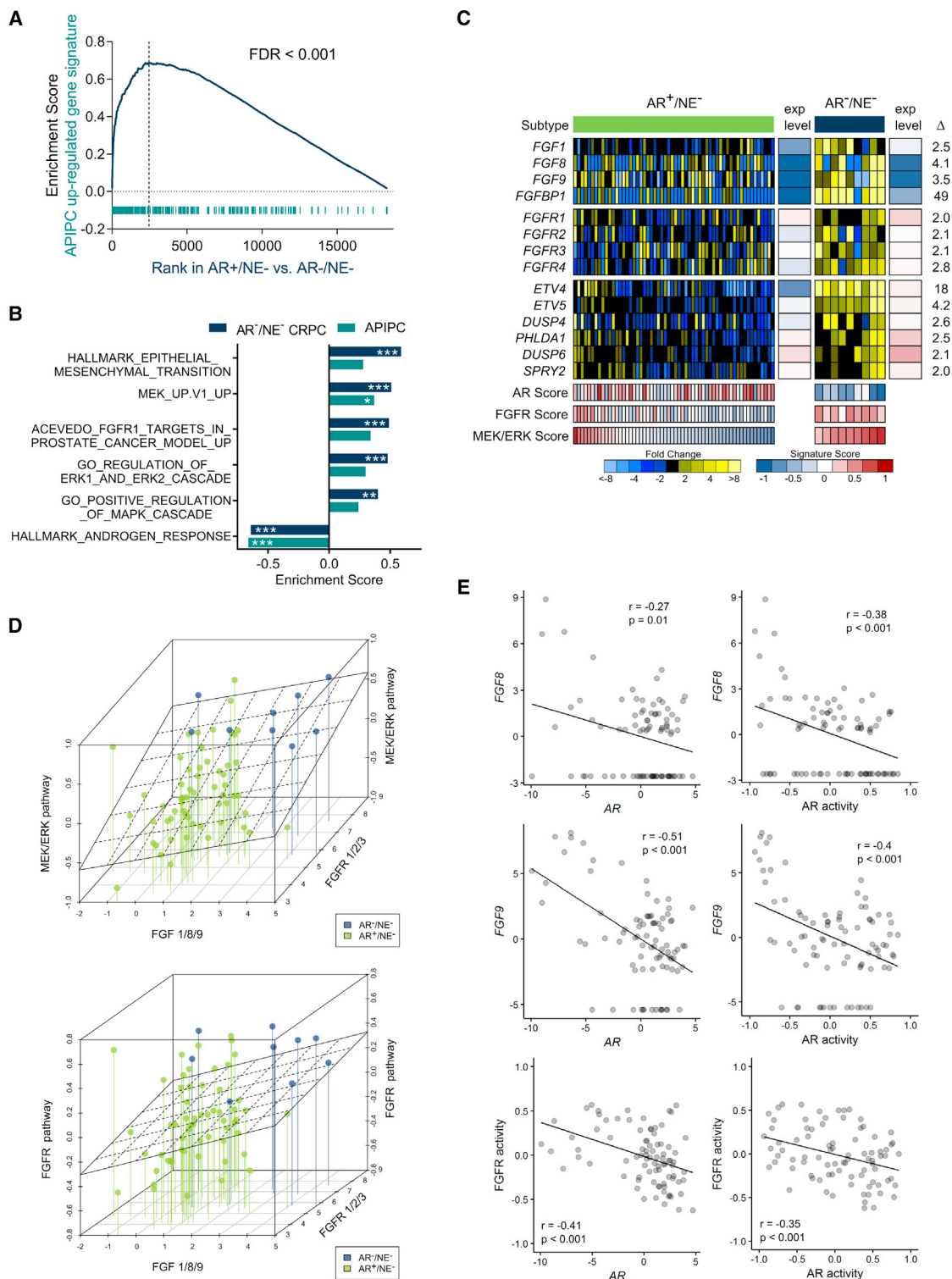


**Figure 4. Assessments of FGF and MAPK Activity in Metastatic CRPC**

(A) Analyses of transcripts differentially expressed between LNCaP<sup>shAR/pATK</sup> and LNCaP<sup>AIPIC</sup> in DNPC and ARPC metastases (FDR < 0.001, pre-ranked GSEA). (B) GSEA demonstrates significant positive associations with FGF, MAPK, MEK/ERK, and EMT pathways and negative enrichment for AR response in DNPC metastases (\*\*\*FDR < 0.0005, \*\*FDR < 0.005, \*FDR < 0.05, pre-ranked GSEA).

(C) Expression of FGF ligands, FGF receptors, and genes comprising an MEK/ERK activity signature. Relative ratios of RNA-seq transcript abundances are shown, along with mean FPKM values and signature scores (AR<sup>+</sup>/NE<sup>-</sup>, n = 58 tumors from 35 men; AR<sup>-</sup>/NE<sup>-</sup>, n = 9 tumors from 5 men).

(legend continued on next page)

with one rib metastasis expressing AR and PSA and a second rib metastasis lacking AR or PSA staining (Figure 5E). We confirmed that the LuCaP173.2 PDX lacks AR and PSA expression and does not express classic NE markers such as chromogranin or synaptophysin, thus fulfilling criteria for DNPC (Figure 5F). However, other genes associated with an NE phenotype such as *EZH2* and *MYCN* are expressed in this PDX line, suggesting a continuum of tumor differentiation (Figure S5). In accord with findings in DNPC metastases, LuCaP173.2 expresses high *FGF9* and *FGFR1* levels with low AR and NEPC program scores and a high FGFR activity score (Figure 5G).

### FGF Activates MAPK Signaling and Bypasses a Requirement for Androgens and the AR in Promoting Prostate Cancer Growth

We next sought to determine whether FGF signaling is necessary and sufficient for bypassing a requirement for AR activity. We hypothesized that the substantial upregulation of FGF8 in LNCaP<sup>APIPC</sup> cells comprises an autocrine loop to sustain cell survival in the absence of AR. The introduction of FGF8-specific small interfering RNAs (siRNAs) reduced LNCaP<sup>APIPC</sup> growth by 80% ( $p < 0.001$ ) (Figure 6A). In contrast, siRNA knockdown of FGF9, which is not upregulated in LNCaP<sup>APIPC</sup>, had no effect. Exogenous FGF8b increased the growth of parental LNCaP<sup>shAR/pATK</sup> in androgen-depleted conditions ( $p < 0.001$ ) and the addition of concentrated LNCaP<sup>APIPC</sup> conditioned medium (CM) showed a small but statistically significant increase in proliferation (11%,  $p = 0.01$ ), whereas LNCaP<sup>shAR/pATK</sup> CM had no effect (Figure 6B). The addition of exogenous FGF8b increased ERK1/2 phosphorylation in both LNCaP<sup>shAR/pATK</sup> and LNCaP<sup>APIPC</sup>. FGF8-induced growth in androgen-depleted conditions and ERK1/2 phosphorylation were blocked by treatment with the FGFR inhibitor PD173074 (Mohammadi et al., 1998) (Figures 6C and 6D).

To demonstrate that FGF8 was sufficient to promote the growth of cells cultured under total AR pathway suppression, we treated parental LNCaP<sup>shAR/pATK</sup> grown in androgen-depleted conditions with Dox to suppress AR expression, and added FGF8b. FGF8b maintained cell proliferation during AR pathway ablation (30% increase in cell number compared with untreated LNCaP<sup>shAR/pATK</sup>;  $p = 0.019$ ), albeit at a lower rate than AR-intact LNCaP<sup>shAR/pATK</sup> (75% increase in cell number compared with untreated LNCaP<sup>shAR/pATK</sup>;  $p = 0.018$ ) (Figure 6E). In a parallel experiment, LNCaP<sup>shAR/pATK</sup> cells were cultured in androgen-depleted medium and AR expression was suppressed by pre-treatment with Dox for 72 hr. Addition of exogenous FGF8b rescued the growth inhibition by ADT and AR suppression (58% increase in growth compared with untreated LNCaP<sup>shAR/pATK</sup>;  $p = 0.003$ ) (Figure S6A).

The FGFR antagonist PD173074 is a nanomolar inhibitor of FGFR1 but is also a submicromolar inhibitor of vascular endothelial growth factor receptor 2/kinase domain receptor (VEGFR2/

KDR) (Mohammadi et al., 1998). To confirm that FGFR antagonism is mediating the growth repression in DNPC, we treated LNCaP<sup>APIPC</sup> with a second FGFR antagonist CH-5183284, which potently and selectively inhibits FGFR1–3 (IC<sub>50</sub> of 8–22 nM) without significant biological effects toward VEGFR2/KDR or other kinases (Nakanishi et al., 2014). At concentrations of 0.1–1.0  $\mu$ M, CH-5183281 substantially inhibited the viability and increased apoptosis rates in LNCaP<sup>APIPC</sup> with effects far exceeding those observed in wild-type LNCaP cells (Figures 6F and 6G). CH-5183281 also reduced the viability of AR-null PacMet-UT1 cells relative to the AR-intact parental line (Figure 6H). Confirming that MAPK activity is required for FGF8-mediated castration-resistant proliferation, the MEK1/2 inhibitor U0126 blocked the growth of LNCaP<sup>shAR/pATK</sup> induced by FGF8 in androgen-depleted conditions ( $p < 0.001$ ; Figure 6I) and repressed LNCaP<sup>APIPC</sup> proliferation. Co-treatment of a second androgen-sensitive PC line, 22RV1, with U0126 and FGF8 led to a 46% decrease in cell number compared with cells treated with FGF8 alone ( $p < 0.001$ ; Figure S6B).

We next sought to determine whether suppressing FGF signaling would inhibit the growth of DNPC *in vivo*. PD173074 significantly reduced LNCaP<sup>APIPC</sup> xenograft growth rates: the study was terminated at 40 days due to large tumors in the control group at which time tumor volumes were 1,147 mm<sup>3</sup> in the vehicle and 571 mm<sup>3</sup> in PD173074 arms ( $p < 0.001$ ) (Figure 6J). To confirm these findings, we treated LuCaP173.2 DNPC PDX tumors with CH-5183284. At the study endpoint of 24 days, tumor volumes were 814 mm<sup>3</sup> and 170 mm<sup>3</sup> in the vehicle and CH-5183284 arms, respectively ( $p < 0.001$ ) (Figure 6K). The expression of FGFR pathway genes as well as composite FGFR and MEK/ERK pathway activity were significantly reduced in LuCaP173.2 tumors resected 3 days and 24 days on CH-5183284 treatment (Figure 6L).

### FGF- and MAPK-Induced ID1 Contributes to AR-Null Prostate Cancer Growth

We next evaluated LNCaP<sup>APIPC</sup> for downstream mediators of FGF/MAPK signaling that could promote the dedifferentiated phenotype of DNPC and support survival in the absence of AR activity. We identified a strong candidate for this role, *inhibitor of differentiation 1 (ID1)*, which was upregulated in LNCaP<sup>APIPC</sup> compared with LNCaP<sup>shAR/pATK</sup> (~10-fold by RNA-seq;  $q < 0.001$ ; 5-fold by qRT-PCR) (Figure 7A). ID1 expression is induced by exogenous FGF and bone morphogenetic protein via MAPK pathway activation (Langenfeld and Langenfeld, 2004; Passiatore et al., 2011), prevents differentiation by binding cell lineage-specific transcription factors (Perk et al., 2005), and has been associated with poorly differentiated PC (Coppe et al., 2004; Sharma et al., 2012). Notably, other ID family members were also increased in LNCaP<sup>APIPC</sup> and the LuCaP173.2 DNPC PDX (Figure 7B). *ID1* levels are significantly higher in DNPC

(D) Plot of CRPC metastasis triangulated by the highest transcript level of FGF1, 8, or 9 (x axis), MEK/ERK pathway activity score or FGFR pathway activity score (y axis), and highest transcript level of FGFR1, 2, or 3 (z axis). Lines anchor MEK/ERK activity to lowest level to assist in visualizing activity on the y axis. A linear regression analysis of pathway score versus ligands and receptors is plotted as a plane (AR<sup>+</sup>/NE<sup>-</sup>,  $n = 58$  tumors from 35 men; AR<sup>-</sup>/NE<sup>-</sup>,  $n = 9$  tumors from 5 men).

(E) Correlation of *FGF8* and *FGF9* transcript levels and FGFR pathway activity and AR activity scores assessed in 85 CRPC metastases from 50 men by RNA-seq. Pearson's correlation coefficient and  $p$  value are indicated on each plot.

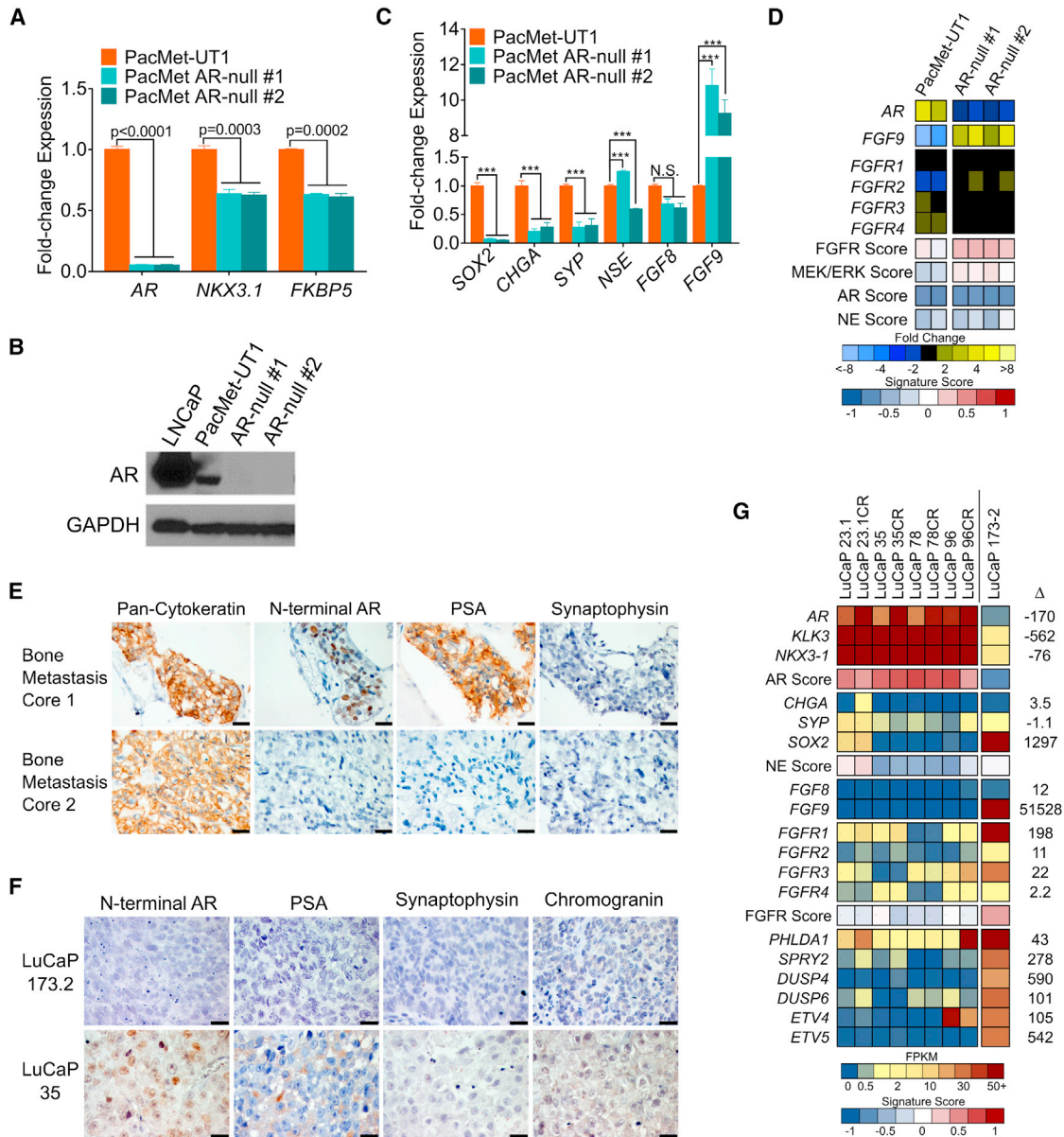


**Figure 5. FGF Pathway and MAPK Activity in Cell Line and PDX Models of DNPC**

(A) Quantitation of the indicated transcripts by qRT-PCR in parental PacMet-UT1 cells and two independent PacMet-UT1 clones propagated after CRISPR/Cas9-mediated AR deletion.

(B) Western immunoblot of AR protein in the indicated cell lines.

(C) Quantitation of the indicated transcripts by qRT-PCR in the indicated cell lines. \*\*\* $p < 0.0001$ . N.S., not significant.

(D) Expression of genes reflecting the activity of AR, neuroendocrine (NE), FGFR, and MAPK signaling in parental PacMet-UT1 cells and AR-null sublines. Measurements were derived from RNA-seq ( $n = 2$  biological replicates per group).

(E) Cytokeratin, AR, PSA, and synaptophysin IHC in two independent rib metastases obtained from a patient with mCRPC. Scale bars, 20  $\mu$ m.

(F) AR, PSA, synaptophysin, and chromogranin IHC in the LuCaP173.2 PDX model derived from rib metastasis core 2 (E) with comparisons with the AR-positive LuCaP35 PDX line. Scale bars, 20  $\mu$ m.

(G) Expression of genes comprising the AR program, neuroendocrine (NE) program, and FGFR program in AR-positive castration-sensitive and castration-resistant (CR) PDX models (LuCaP23.1, LuCaP35, LuCaP78, and LuCaP96) and the AR-null, NE-null LuCaP173.2 PDX line. Measurements were derived from RNA-seq ( $n =$  one tumor from each LuCaP line).

For (A) and (C), significance was determined by Student's  $t$  test and data are presented as mean  $\pm$  SEM ( $n = 3$  replicates per data point). See also Figure S5.

metastases relative to ARPCs ( $p < 0.005$ ) (Figure 7C), and ID1 and AR expression are inversely associated in mCRPC (Pearson correlation =  $-0.39$ ) (Figure 7D).

Stimulation of LNCaP<sup>shAR/pATK</sup> cells with FGF8 resulted in a 4-fold ( $p = 0.006$ ) increase in ID1 mRNA and protein (Figures 7E and 7F). MEK inhibition reduced FGF8-mediated

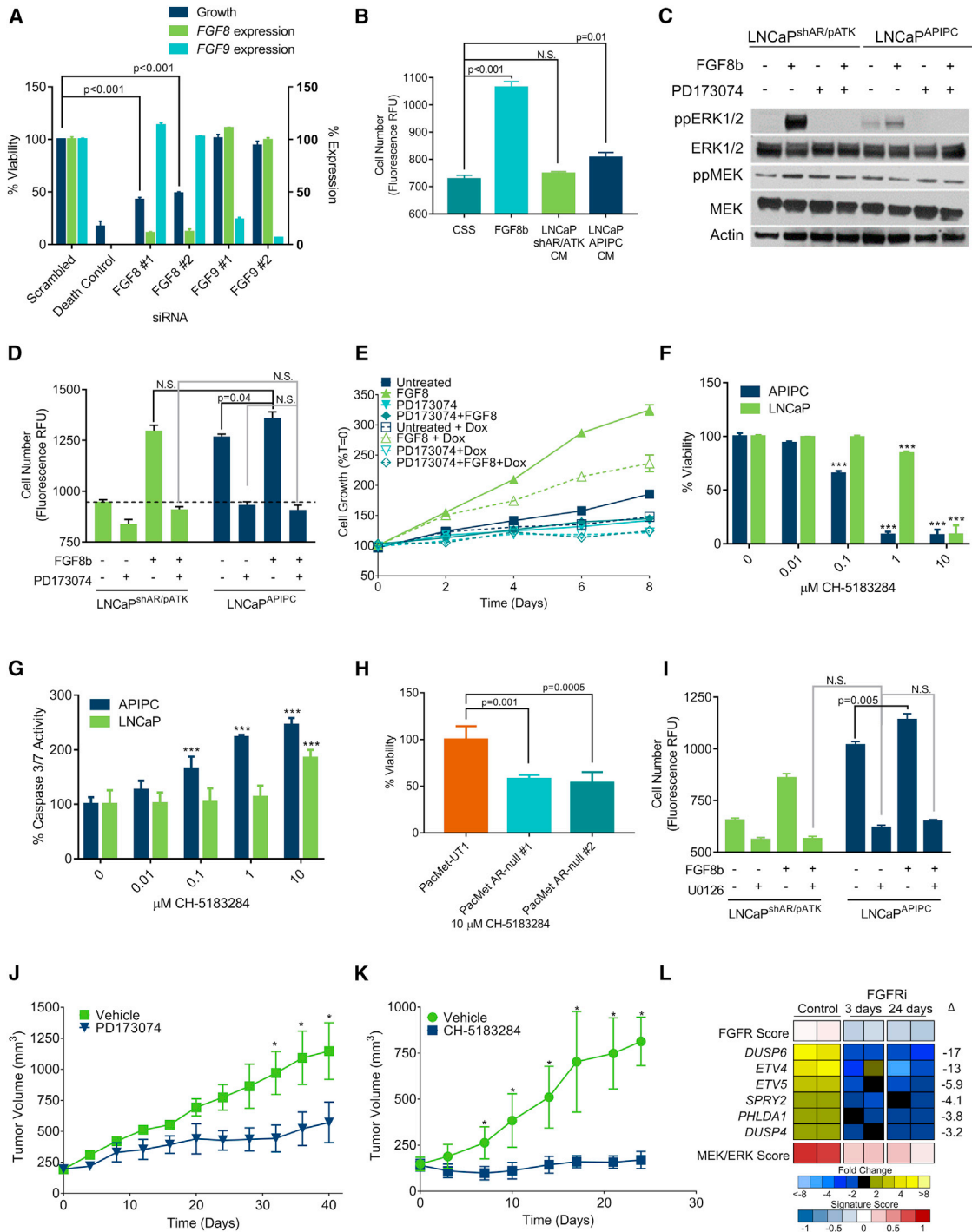


**Figure 6. FGF Activates MAPK Signaling and Bypasses a Requirement for AR Activity in Promoting Prostate Cancer Growth**

(A) Quantitation of cell viability and gene expression 96 hr after transfecting LNCaP<sup>APIPC</sup> cells with siRNA pools specific for the indicated target. (B) LNCaP<sup>shAR/pATK</sup> were cultured for 4 days in androgen-depleted medium and treated with 25 ng/mL FGF8b, CM from LNCaP<sup>shAR/pATK</sup>, or LNCaP<sup>APIPC</sup> cells. Cell number was determined using Cyquant. (C) LNCaP<sup>shAR/pATK</sup> and LNCaP<sup>APIPC</sup> were treated with 1 μM PD173074 or vehicle and 25 ng/mL FGF8 or vehicle and cell lysates were evaluated for MAPK signaling via immunoblotting for ppERK1/2. (D) LNCaP<sup>shAR/pATK</sup> and LNCaP<sup>APIPC</sup> were cultured in androgen-depleted conditions and treated with ±25 ng/mL FGF8b and ±1 μM PD173074. N.S., not significant. Dashed line indicates unstimulated LNCaP<sup>shAR/pATK</sup> (n = 3 replicates per data point). (E) LNCaP<sup>shAR/pATK</sup> cells were cultured in androgen-depleted medium ±25 ng/mL FGF8, ±1 μM PD173074, and ±1 μg/mL Dox. Solid lines, no Dox; dotted lines, with Dox. Cell number was determined using Cyquant, and values were normalized to day 0. (legend continued on next page)

ID1 induction by approximately 30% ( $p = 0.005$ ) (Figure 7E). Although ID1 levels were already elevated, stimulation of LNCaP<sup>APIPC</sup> with exogenous FGF8 resulted in a further 1.6-fold increase ( $p < 0.001$ ), and treatment with U0126 alone decreased baseline ID1 expression by approximately 40% ( $p = 0.006$ ) (Figure 7E). We also observed a significant upregulation of ID1 in response to FGF8 treatment in androgen-sensitive 22Rv1 cells (Figures S7A and S7B). The enhanced activity of specific RTKs is associated with ligand-independent activation of AR transcription in some models (Gregory et al., 2005; Yang et al., 2003); however, we did not observe a change in AR, PSA, or TMPRSS2 expression in response to FGF8b stimulation in androgen-deprived LNCaP<sup>shAR/pATK</sup>, LNCaP<sup>APIPC</sup>, or 22Rv1 cells (Figures 7G and S7C).

ID1 has been shown to influence PC differentiation and proliferation (Ling et al., 2011; Ouyang et al., 2002), and we hypothesized that ID1 could mediate a component of the growth-promoting effects of FGF/MAPK activity. In support of this hypothesis, levels of ID1–3 transcripts were diminished in the LuCaP173.2 DNPC PDX tumors treated with the FGFR inhibitor CH-5183284 (Figure 7H). ID1 knockdown did not significantly affect LNCaP<sup>shAR/pATK</sup> growth compared with a scrambled control siRNA (siUNI). In contrast, two independent ID1-targeting siRNAs decreased LNCaP<sup>APIPC</sup> growth by 32% ( $p = 0.003$ ) and 43% ( $p < 0.001$ ) (Figure 7I). When LNCaP<sup>shAR/pATK</sup> were treated with FGF8, ID1 knockdown significantly attenuated FGF8-induced proliferation by ~35% ( $p < 0.001$ ). The effect of ID1 knockdown was enhanced in LNCaP<sup>APIPC</sup> with ID1 siRNAs suppressing FGF8-induced growth by 39%–50% ( $p < 0.001$ ) (Figure 7I). These effects were replicated in 22RV1 cells grown in androgen-deprived conditions (Figure S7D).

## DISCUSSION

Therapeutic approaches designed to impair AR activity remain first-line therapy for men with metastatic PC. While resistance to AR-directed therapeutics is usually accompanied by reactivation of AR signaling, newer drugs with potent AR pathway antagonism appear to be shifting the phenotypes of resistant PC to anaplastic and NE carcinomas that are devoid of AR activity (Figure 7J). The AR-null/NE-null tumors evaluated in the present study were acquired from men after initial responses to AR antagonists, indicating that these agents effectively eliminated tumor clones dependent on the AR, but failed to eradicate cell populations that no longer required AR signaling. Defining the

drivers of these resistant carcinomas is critical for the development of effective treatment strategies.

We determined that complete AR pathway independence was associated with elevated autocrine FGF signaling *in vitro* and elevated FGFR and MAPK pathway activity in mCRPC. FGF ligands and receptors have previously been shown to influence the development and progression of PC (Acedo et al., 2007; Feng et al., 2015). Of relevance to the present study, a PDX model of PC devoid of AR signaling was shown to express high levels of FGF9, which promoted tumor growth, induced an osteoblastic tumor microenvironment, and responded to FGF-directed therapy (Li et al., 2008). MAPK signaling promotes poorly differentiated tumor growth in models of PC (Mulholland et al., 2012), and constitutive ERK1/2 activity is associated with castration resistance (Gioeli et al., 1999; Oka et al., 2005; Rodriguez-Berriguete et al., 2012). While there is evidence suggesting that MAPK can stimulate ligand-independent AR activity (Feldman and Feldman, 2001), FGF/MAPK signaling did not promote the re-expression of AR-regulated genes in our models and FGFR activity was inversely associated with the expression and activity of AR in CRPCs. At this time, the mechanism(s) influencing FGF expression in LNCaP<sup>APIPC</sup> or other DNPCs is not known. As we found no recurrent genomic events involving FGFs/FGFRs, other processes capable of influencing FGF transcription, including epigenetic regulation, are likely operative. Notably, a small subset of CRPCs exhibiting FGFR/MAPK activity did not express high levels of FGF ligands, suggesting that in some circumstances paracrine FGF derived from microenvironment constituents may promote pathway activity and drive treatment resistance (Lawson et al., 2010).

While AR repression can allow for cellular reprogramming and transdifferentiation to NE carcinoma (Ku et al., 2017; Zou et al., 2017), our results indicate that the acquisition of NE characteristics may represent a continuum of differentiation from ARPC to DNPC to NEPC, although the acquisition of NE characteristics does not appear to be a certainty following AR ablation (Figure 7J). Importantly, alternative cell fates may associate with unique therapeutic vulnerabilities. Given that NE and anaplastic tumors are more common following sustained AR pathway suppression and appear to arise from adenocarcinomas *in vivo* based on shared genomic aberrations (Beltran et al., 2011, 2016), it is quite likely that the incidence of AR pathway-independent PCs will increase with the deployment of increasingly potent AR inhibition. Whether acute and more complete AR

(F and G) LNCaP and LNCaP<sup>APIPC</sup> were treated with the indicated concentrations of CH-5183284, and cell viability (F) and apoptosis (G) were measured after 72 hr by ApoLive Glo ( $n = 3$  replicates per data point). \*\*\* $p < 0.001$ .

(H) PacMet-UT1 cells and AR-null derivatives were treated with 10  $\mu$ M CH-5183284, and cell viability was determined by CellTiter Glo after 72 hr.

(I) LNCaP<sup>shAR/pATK</sup> and LNCaP<sup>APIPC</sup> cultured in androgen-depleted conditions were treated with FGF8b or vehicle with or without 25  $\mu$ M U0126 or vehicle. Cell number was determined using Cyquant.

(J) LNCaP<sup>APIPC</sup> cells were inoculated subcutaneously in castrate SCID mice receiving Dox-supplemented feed. When tumors reached 200 mm<sup>3</sup> in size, treatment was initiated with the FGFR antagonist PD173074 or vehicle control. Tumor volumes were measured every 2 days ( $n = 5$ ). \* $p < 0.01$ .

(K) LuCaP173.2 tumors were implanted subcutaneously in castrate SCID mice. When tumors reached 200 mm<sup>3</sup> in size, treatment was initiated with the FGFR antagonist CH-5183284 or vehicle control. Tumor volumes were measured every 2 days ( $n = 15$ ). \* $p < 0.01$ .

(L) Quantitation of FGFR and MEK/ERK pathway gene expression in LuCaP173.2 tumors treated with vehicle or CH-5183284 sampled 3 days or 24 days after the initiation of treatment. Transcripts were quantitated by RNA-seq of two independent tumors. Significance was determined by Student's *t* test and data are presented as mean  $\pm$  SEM.

For (A), (B), and (D) to (I),  $n = 3$  replicates per data point. See also Figure S6.

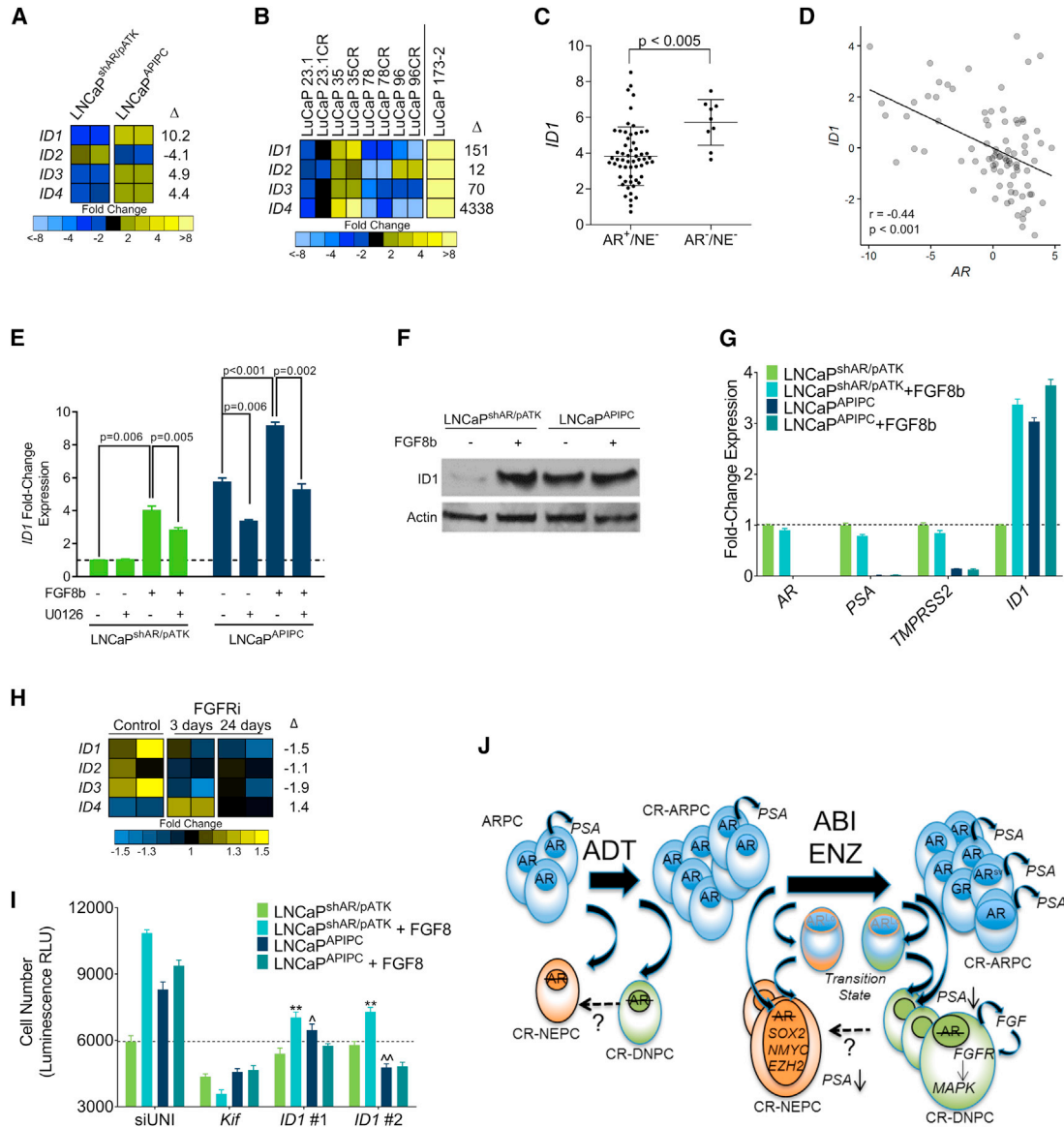


**Figure 7. FGF8 Induces ID1 Expression and Castration-Resistant Growth via MAPK Pathway Activation**

(A) Transcript levels of *ID1-4* in LNCaP<sup>shAR/pATK</sup> and LNCaP<sup>APIPC</sup> cells determined by RNA-seq in two independent cultures. Fold differences of gene expression levels between LNCaP<sup>shAR/pATK</sup> and LNCaP<sup>APIPC</sup> cells are shown.

(B) Expression of *ID1-4* in AR-positive castration-sensitive and castration-resistant (CR) PDX models (LuCaP23.1, LuCaP35, LuCaP78, and LuCaP96) and the AR-null, NE-null LuCaP173.2 PDX line. Measurements were derived from RNA-seq (n = one tumor from each LuCaP line). Fold differences of gene expression between AR-positive and AR-negative groups are shown.

(C) Transcript levels of *ID1* in AR<sup>+</sup>/NE<sup>-</sup> and AR<sup>-</sup>/NE<sup>-</sup> CRPC metastases determined by RNA-seq transcript quantitation. Log<sup>2</sup> counts per million (CPM) mapped reads with mean ± SD are plotted. Groups were compared by unpaired, two-tailed t test (AR<sup>+</sup>/NE<sup>-</sup>, n = 58 tumors from 35 men; AR<sup>-</sup>/NE<sup>-</sup>, n = 9 tumors from 5 men).

(D) Association of *ID1* and *AR* transcripts in CRPC metastases. Each data point represents an individual metastasis (n = 85 tumors from 50 men). Transcript levels were quantitated by RNA-seq. Pearson's correlation coefficient r = -0.39; p < 0.001.

(E) *ID1* transcripts quantitated by qRT-PCR in LNCaP<sup>shAR/pATK</sup> and LNCaP<sup>APIPC</sup> treated with 25 ng/mL FGF8 or vehicle and the MEK inhibitor U0126 or vehicle. qRT-PCR values were normalized to RPL13a expression, and compared with unstimulated LNCaP<sup>shAR/pATK</sup>.

(F) Immunoblot of cell lysates collected from LNCaP<sup>shAR/pATK</sup> and LNCaP<sup>APIPC</sup> treated with 25 ng/mL FGF8 or vehicle probed with anti-ID1 antibody.

(G) LNCaP<sup>shAR/pATK</sup> and LNCaP<sup>APIPC</sup> were cultured under androgen-depleted conditions and treated with vehicle (PBS) or 25 ng/mL FGF8. *ID1*, *AR*, *PSA*, and *TMPRSS2* transcripts were quantitated by qRT-PCR, normalized to *RPL13a* expression, and compared with unstimulated LNCaP<sup>shAR/pATK</sup>.

(H) Quantitation of *ID1-4* in LuCaP173.2 tumors treated with vehicle or CH-5183284 sampled 3 days or 24 days after the initiation of treatment. Transcripts were quantitated by RNA-seq of two independent tumors.

(legend continued on next page)

repression will eliminate PCs or consistently generate AR-null variants remains to be determined. Early results from an ongoing clinical trial (NCT00831792) of the FGFR antagonist dovitinib in men with metastatic CRPC unselected for loss of AR activity reported a 26% response rate in bone and soft tissue lesions (Wan et al., 2014). Our results suggest that FGFR inhibition may have modest effects in AR-active CRPCs, but be particularly active in the subset of CRPCs with absent or limited AR function. A clinical trial of FGFR or MAPK antagonists may be fruitful in patients stratified by AR activity status. Furthermore, co-targeting of predictable AR bypass pathways capable of providing robust cell survival and proliferation signals may prolong responses to initial AR antagonism.

## STAR★METHODS

Detailed methods are provided in the online version of this paper and include the following:

- KEY RESOURCES TABLE
- LEAD CONTACT FOR REAGENT AND RESOURCE SHARING
- EXPERIMENTAL MODELS AND SUBJECT DETAILS
  - Cell Lines
  - Tissue Acquisition
  - LNCaP<sup>APIPC</sup> Xenograft Mouse Models
  - PDX Mouse Models
- METHOD DETAILS
  - Cell Culture
  - Migration and Invasion Assays
  - Cell Growth Assays
  - Conditioned Media
  - siRNA Transfection
  - RNA Collection and Quantitative Real-Time PCR
  - Protein Collection and Immunoblotting
  - Immunohistochemistry
  - AR CRISPR-Cas9 Editing
  - Transcript Profiling Methods
- QUANTIFICATION AND STATISTICAL ANALYSIS
- DATA AND SOFTWARE AVAILABILITY

## SUPPLEMENTAL INFORMATION

Supplemental Information includes seven figures and one table and can be found with this article online at <http://dx.doi.org/10.1016/j.ccell.2017.09.003>.

## AUTHOR CONTRIBUTIONS

P.S.N., E.G.B., and C.M. conceived the project; E.G.B., S.H.-L., E.C., and H.M.N. performed mouse experiments; I.M.C., R.T.C., A.K., R.T., and D.W. performed sequencing and bioinformatics analyses; E.G.B., J.M.L., D.B.-F., R.F.D., A.N.C., Y.C.Y., M.D.N., and L.G.B. conducted molecular and cell biology experiments; X.Z., L.D.T., and M.I. provided pathology evaluation;

E.M., A.H., M.S., K.P., R.L.V., and P.S.R. provided biospecimens, model systems, and clinical expertise; P.S.N., I.M.C., and C.M. wrote the manuscript; all authors reviewed and edited the manuscript.

## ACKNOWLEDGMENTS

We are grateful to the patients and their families who participated in this study. We thank members of the P.S.N. laboratory for helpful advice and criticism. We thank Steve Plymate for helpful advice and assistance with analyses. We thank the FHCRC Genomics shared resource for assistance with RNA-seq experiments. We would also like to thank Yoshito Nakanishi for his advice, Bryce Lakely and Belinda Nguyen for technical assistance, Celestia Higano, Bruce Montgomery, Evan Yu, Heather Cheng, Funda-Vakar Lopez, Martine Roudier, Kristine Von Maltzan, Maria Tretiakova, and the rapid autopsy teams in the Urology Department at the University of Washington for their contributions to the Prostate Cancer Donor Rapid Autopsy Program. This work was supported by NIH awards: Prostate SPORE grant P50CA097186, P01 CA163227, DOD awards PC140794 and PC160662, a DF/HCC Mazzone award, the Institute for Prostate Cancer Research, the Richard M. Lucas Foundation, and a Challenge award from Movember and the Prostate Cancer Foundation.

Received: June 18, 2017

Revised: August 1, 2017

Accepted: September 5, 2017

Published: October 9, 2017

## REFERENCES

- Acevedo, V.D., Gangula, R.D., Freeman, K.W., Li, R., Zhang, Y., Wang, F., Ayala, G.E., Peterson, L.E., Ittmann, M., and Spencer, D.M. (2007). Inducible FGFR-1 activation leads to irreversible prostate adenocarcinoma and an epithelial-to-mesenchymal transition. *Cancer Cell* 12, 559–571.
- Aihara, M., Lebovitz, R.M., Wheeler, T.M., Kinner, B.M., Otori, M., and Scardino, P.T. (1994). Prostate specific antigen and Gleason grade: an immunohistochemical study of prostate cancer. *J. Urol.* 151, 1558–1564.
- Aparicio, A., Tzelepi, V., Araujo, J.C., Guo, C.C., Liang, S., Troncoso, P., Logothetis, C.J., Navone, N.M., and Maity, S.N. (2011). Neuroendocrine prostate cancer xenografts with large-cell and small-cell features derived from a single patient's tumor: morphological, immunohistochemical, and gene expression profiles. *Prostate* 71, 846–856.
- Arora, V.K., Schenkein, E., Murali, R., Subudhi, S.K., Wongvipat, J., Balbas, M.D., Shah, N., Cai, L., Efstathiou, E., Logothetis, C., et al. (2013). Glucocorticoid resistance confers resistance to antiandrogens by bypassing androgen receptor blockade. *Cell* 155, 1309–1322.
- Aytes, A., Mitrofanova, A., Kinkade, C.W., Lefebvre, C., Lei, M., Phelan, V., LeKaye, H.C., Koutcher, J.A., Cardiff, R.D., Califano, A., et al. (2013). ETV4 promotes metastasis in response to activation of PI3-kinase and Ras signaling in a mouse model of advanced prostate cancer. *Proc. Natl. Acad. Sci. USA* 110, E3506–E3515.
- Beltran, H., Prandi, D., Mosquera, J.M., Benelli, M., Puca, L., Cyrta, J., Marotz, C., Giannopoulou, E., Chakravarthi, B.V., Varambally, S., et al. (2016). Divergent clonal evolution of castration-resistant neuroendocrine prostate cancer. *Nat. Med.* 22, 298–305.
- Beltran, H., Rickman, D.S., Park, K., Chae, S.S., Sboner, A., MacDonald, T.Y., Wang, Y., Sheikh, K.L., Terry, S., Tagawa, S.T., et al. (2011). Molecular characterization of neuroendocrine prostate cancer and identification of new drug targets. *Cancer Discov.* 1, 487–495.

(I) LNCaP<sup>shAR/pATK</sup> and LNCaP<sup>APIPC</sup> were cultured in androgen-depleted medium and transfected with siRNA specific for target genes. Cells were treated with 25 ng/mL FGF8 or vehicle. siUNI, non-targeting control siRNA; Kif11, equimolar mixture of three siRNAs targeting Kif11 and a positive control for transfection efficiency; ID1 #1 and ID1 #2 are siRNAs targeting ID1. Relative cellular number was measured with the Cell Titer Glo luminescence assay.

(J) Schematic depicting the cellular differentiation states and underlying molecular drivers of cell survival and growth following AR pathway-directed therapy. ADT, androgen deprivation therapy; ABI, abiraterone; ENZ, enzalutamide; CR-ARPC, castration-resistant AR program active PC; CR-NEPC, castration-resistant NE program active PC; CR-DNPC, castration-resistant PC without AR or NE program activity.

For (E), (G), and (I), significance was determined by Student's t test and data are presented as mean ± SEM (n = 3–5 replicates per data point). See also Figure S7.

- Beltran, H., Tomlins, S., Aparicio, A., Arora, V., Rickman, D., Ayala, G., Huang, J., True, L., Gleave, M.E., Soule, H., et al. (2014). Aggressive variants of castration-resistant prostate cancer. *Clin. Cancer Res.* **20**, 2846–2850.
- Carver, B.S., Chapinski, C., Wongvipat, J., Hieronymus, H., Chen, Y., Chandralapaty, S., Arora, V.K., Le, C., Koutcher, J., Scher, H., et al. (2011). Reciprocal feedback regulation of PI3K and androgen receptor signaling in PTEN-deficient prostate cancer. *Cancer Cell* **19**, 575–586.
- Cheng, H., Snoek, R., Ghaidi, F., Cox, M.E., and Rennie, P.S. (2006). Short hairpin RNA knockdown of the androgen receptor attenuates ligand-independent activation and delays tumor progression. *Cancer Res.* **66**, 10613–10620.
- Coppe, J.P., Itahana, Y., Moore, D.H., Bennington, J.L., and Desprez, P.Y. (2004). Id-1 and Id-2 proteins as molecular markers for human prostate cancer progression. *Clin. Cancer Res.* **10**, 2044–2051.
- de Bono, J.S., Logothetis, C.J., Molina, A., Fizazi, K., North, S., Chu, L., Chi, K.N., Jones, R.J., Goodman, O.B., Jr., Saad, F., et al. (2011). Abiraterone and increased survival in metastatic prostate cancer. *N. Engl. J. Med.* **364**, 1995–2005.
- Delpuech, O., Rooney, C., Mooney, L., Baker, D., Shaw, R., Dymond, M., Wang, D., Zhang, P., Cross, S., Veldman-Jones, M., et al. (2016). Identification of pharmacodynamic transcript biomarkers in response to FGFR inhibition by AZD4547. *Mol. Cancer Ther.* **15**, 2802–2813.
- Doctor, S.M., Tsao, C.K., Godbold, J.H., Galsky, M.D., and Oh, W.K. (2014). Is prostate cancer changing?: evolving patterns of metastatic castration-resistant prostate cancer. *Cancer* **120**, 833–839.
- Erbersdobler, A., Isbarn, H., Steiner, I., Schlomm, T., Chun, F., Mirlacher, M., and Sauter, G. (2009). Predictive value of prostate-specific antigen expression in prostate cancer: a tissue microarray study. *Urology* **74**, 1169–1173.
- Feldman, B.J., and Feldman, D. (2001). The development of androgen-independent prostate cancer. *Nat. Rev. Cancer* **1**, 34–45.
- Feng, S., Wang, J., Zhang, Y., Creighton, C.J., and Ittmann, M. (2015). FGF23 promotes prostate cancer progression. *Oncotarget* **6**, 17291–17301.
- Gioeli, D., Mandell, J.W., Petroni, G.R., Frierson, H.F., Jr., and Weber, M.J. (1999). Activation of mitogen-activated protein kinase associated with prostate cancer progression. *Cancer Res.* **59**, 279–284.
- Gregory, C.W., Whang, Y.E., McCall, W., Fei, X., Liu, Y., Ponguta, L.A., French, F.S., Wilson, E.M., and Earp, H.S., 3rd (2005). Heregulin-induced activation of HER2 and HER3 increases androgen receptor transactivation and CWR-R1 human recurrent prostate cancer cell growth. *Clin. Cancer Res.* **11**, 1704–1712.
- Hänzelmann, S., Castelo, R., and Guinney, J. (2013). GSEA: gene set variation analysis for microarray and RNA-seq data. *BMC Bioinformatics* **14**, 7.
- Hieronymus, H., Lamb, J., Ross, K.N., Peng, X.P., Clement, C., Rodina, A., Nieto, M., Du, J., Stegmaier, K., Raj, S.M., et al. (2006). Gene expression signature-based chemical genomic prediction identifies a novel class of HSP90 pathway modulators. *Cancer Cell* **10**, 321–330.
- Kim, D., Perte, G., Trapnell, C., Pimentel, H., Kelley, R., and Salzberg, S.L. (2013). TopHat2: accurate alignment of transcriptomes in the presence of insertions, deletions and gene fusions. *Genome Biol.* **14**, R36.
- Ku, S.Y., Rosario, S., Wang, Y., Mu, P., Seshadri, M., Goodrich, Z.W., Goodrich, M.M., Labbe, D.P., Gomez, E.C., Wang, J., et al. (2017). Rb1 and Trp53 cooperate to suppress prostate cancer lineage plasticity, metastasis, and antiandrogen resistance. *Science* **355**, 78–83.
- Kumar, A., Coleman, I., Morrissey, C., Zhang, X., True, L.D., Gulati, R., Etzioni, R., Bolouri, H., Montgomery, B., White, T., et al. (2016). Substantial interindividual and limited intraindividual genomic diversity among tumors from men with metastatic prostate cancer. *Nat. Med.* **22**, 369–378.
- Langenfeld, E.M., and Langenfeld, J. (2004). Bone morphogenetic protein-2 stimulates angiogenesis in developing tumors. *Mol. Cancer Res.* **2**, 141–149.
- Lawrence, M., Huber, W., Pagès, H., Aboyoun, P., Carlson, M., Gentleman, R., Morgan, M.T., and Carey, V.J. (2013). Software for computing and annotating genomic ranges. *PLoS Comput. Biol.* **9**, e1003118.
- Lawson, D.A., Zong, Y., Memarzadeh, S., Xin, L., Huang, J., and Witte, O.N. (2010). Basal epithelial stem cells are efficient targets for prostate cancer initiation. *Proc. Natl. Acad. Sci. USA* **107**, 2610–2615.
- Li, Z.G., Mathew, P., Yang, J., Starbuck, M.W., Zurita, A.J., Liu, J., Sikes, C., Multani, A.S., Efstathiou, E., Lopez, A., et al. (2008). Androgen receptor-negative human prostate cancer cells induce osteogenesis in mice through FGF9-mediated mechanisms. *J. Clin. Invest.* **118**, 2697–2710.
- Ligges, U., and Machler, M. (2003). Scatterplot3d: an R package for visualizing multivariate data. *J. Stat. Softw.* **8**, 1–20.
- Ling, Y.X., Tao, J., Fang, S.F., Hui, Z., and Fang, Q.R. (2011). Downregulation of Id1 by small interfering RNA in prostate cancer PC3 cells in vivo and in vitro. *Eur. J. Cancer Prev.* **20**, 9–17.
- MacArthur, C.A., Lawshe, A., Shankar, D.B., Heikinheimo, M., and Shackelford, G.M. (1995). FGF-8 isoforms differ in NIH3T3 cell transforming potential. *Cell Growth Differ.* **6**, 817–825.
- Mohammadi, M., Froum, S., Hamby, J.M., Schroeder, M.C., Panek, R.L., Lu, G.H., Eliseenkova, A.V., Green, D., Schlessinger, J., and Hubbard, S.R. (1998). Crystal structure of an angiogenesis inhibitor bound to the FGF receptor tyrosine kinase domain. *EMBO J.* **17**, 5896–5904.
- Montgomery, R.B., Mostaghel, E.A., Vessella, R., Hess, D.L., Kalhorn, T.F., Higoano, C.S., True, L.D., and Nelson, P.S. (2008). Maintenance of intratumoral androgens in metastatic prostate cancer: a mechanism for castration-resistant tumor growth. *Cancer Res.* **68**, 4447–4454.
- Mu, P., Zhang, Z., Benelli, M., Karthaus, W.R., Hoover, E., Chen, C.C., Wongvipat, J., Ku, S.Y., Gao, D., Cao, Z., et al. (2017). SOX2 promotes lineage plasticity and antiandrogen resistance in TP53- and RB1-deficient prostate cancer. *Science* **355**, 84–88.
- Mulholland, D.J., Kobayashi, N., Ruscetti, M., Zhi, A., Tran, L.M., Huang, J., Gleave, M., and Wu, H. (2012). Pten loss and RAS/MAPK activation cooperate to promote EMT and metastasis initiated from prostate cancer stem/progenitor cells. *Cancer Res.* **72**, 1878–1889.
- Mulholland, D.J., Tran, L.M., Li, Y., Cai, H., Morim, A., Wang, S., Plaisier, S., Garraway, I.P., Huang, J., Graeber, T.G., and Wu, H. (2011). Cell autonomous role of PTEN in regulating castration-resistant prostate cancer growth. *Cancer Cell* **19**, 792–804.
- Nakanishi, Y., Akiyama, N., Tsukaguchi, T., Fujii, T., Sakata, K., Sase, H., Isobe, T., Morikami, K., Shindoh, H., Mio, T., et al. (2014). The fibroblast growth factor receptor genetic status as a potential predictor of the sensitivity to CH5183284/Debio 1347, a novel selective FGFR inhibitor. *Mol. Cancer Ther.* **13**, 2547–2558.
- Nelson, P.S., Clegg, N., Arnold, H., Ferguson, C., Bonham, M., White, J., Hood, L., and Lin, B. (2002). The program of androgen-responsive genes in neoplastic prostate epithelium. *Proc. Natl. Acad. Sci. USA* **99**, 11890–11895.
- Oka, H., Chatani, Y., Kohno, M., Kawakita, M., and Ogawa, O. (2005). Constitutive activation of the 41- and 43-kDa mitogen-activated protein (MAP) kinases in the progression of prostate cancer to an androgen-independent state. *Int. J. Urol.* **12**, 899–905.
- Ouyang, X.S., Wang, X., Ling, M.T., Wong, H.L., Tsao, S.W., and Wong, Y.C. (2002). Id-1 stimulates serum independent prostate cancer cell proliferation through inactivation of p16(INK4a)/pRB pathway. *Carcinogenesis* **23**, 721–725.
- Paradis, E., Claude, J., and Strimmer, K. (2004). APE: analyses of phylogenetics and evolution in R language. *Bioinformatics* **20**, 289–290.
- Passiatore, G., Gentilella, A., Rom, S., Pacifici, M., Bergonzini, V., and Peruzzi, F. (2011). Induction of Id-1 by FGF-2 involves activity of EGR-1 and sensitizes neuroblastoma cells to cell death. *J. Cell Physiol.* **226**, 1763–1770.
- Perk, J., Iavarone, A., and Benezra, R. (2005). Id family of helix-loop-helix proteins in cancer. *Nat. Rev. Cancer* **5**, 603–614.
- Robinson, M.D., McCarthy, D.J., and Smyth, G.K. (2010). edgeR: a Bioconductor package for differential expression analysis of digital gene expression data. *Bioinformatics* **26**, 139–140.
- Robinson, D., Van Allen, E.M., Wu, Y.M., Schultz, N., Lonigro, R.J., Mosquera, J.M., Montgomery, B., Taplin, M.E., Pritchard, C.C., Attard, G., et al. (2015). Integrative clinical genomics of advanced prostate cancer. *Cell* **161**, 1215–1228.

- Rodríguez-Berriguete, G., Fraile, B., Martínez-Onsurbe, P., Olmedilla, G., Paniagua, R., and Royuela, M. (2012). MAP kinases and prostate cancer. *J. Signal. Transduct.* *2012*, 169170.
- Roudier, M.P., True, L.D., Higano, C.S., Vessella, H., Ellis, W., Lange, P., and Vessella, R.L. (2003). Phenotypic heterogeneity of end-stage prostate carcinoma metastatic to bone. *Hum. Pathol.* *34*, 646–653.
- Sanjana, N.E., Shalem, O., and Zhang, F. (2014). Improved vectors and genome-wide libraries for CRISPR screening. *Nat. Methods* *11*, 783–784.
- Scher, H.I., Fizazi, K., Saad, F., Taplin, M.E., Sternberg, C.N., Miller, K., de Wit, R., Mulders, P., Chi, K.N., Shore, N.D., et al. (2012). Increased survival with enzalutamide in prostate cancer after chemotherapy. *N. Engl. J. Med.* *367*, 1187–1197.
- Shah, R.B., Mehra, R., Chinnaiyan, A.M., Shen, R., Ghosh, D., Zhou, M., Macvicar, G.R., Varambally, S., Harwood, J., Bismar, T.A., et al. (2004). Androgen-independent prostate cancer is a heterogeneous group of diseases: lessons from a rapid autopsy program. *Cancer Res.* *64*, 9209–9216.
- Sharma, P., Patel, D., and Chaudhary, J. (2012). Id1 and Id3 expression is associated with increasing grade of prostate cancer: Id3 preferentially regulates CDKN1B. *Cancer Med.* *1*, 187–197.
- Snoek, R., Cheng, H., Margiotti, K., Wafa, L.A., Wong, C.A., Wong, E.C., Fazli, L., Nelson, C.C., Gleave, M.E., and Rennie, P.S. (2009). In vivo knockdown of the androgen receptor results in growth inhibition and regression of well-established, castration-resistant prostate tumors. *Clin. Cancer Res.* *15*, 39–47.
- Sobel, R.E., and Sadar, M.D. (2005). Cell lines used in prostate cancer research: a compendium of old and new lines—part 2. *J. Urol.* *173*, 360–372.
- Subramanian, A., Tamayo, P., Mootha, V.K., Mukherjee, S., Ebert, B.L., Gillette, M.A., Paulovich, A., Pomeroy, S.L., Golub, T.R., Lander, E.S., et al. (2005). Gene set enrichment analysis: a knowledge-based approach for interpreting genome-wide expression profiles. *Proc. Natl. Acad. Sci. USA* *102*, 15545–15550.
- Taylor, B.S., Schultz, N., Hieronymus, H., Gopalan, A., Xiao, Y., Carver, B.S., Arora, V.K., Kaushik, P., Cerami, E., Reva, B., et al. (2010). Integrative genomic profiling of human prostate cancer. *Cancer Cell* *18*, 11–22.
- Troyer, D.A., Tang, Y., Bedolla, R., Adhvaryu, S.G., Thompson, I.M., Abboud-Werner, S., Sun, L.Z., Friedrichs, W.E., and deGraffenried, L.A. (2008). Characterization of PacMetUT1, a recently isolated human prostate cancer cell line. *Prostate* *68*, 883–892.
- Tzelepi, V., Zhang, J., Lu, J.F., Kleb, B., Wu, G., Wan, X., Hoang, A., Efstathiou, E., Sircar, K., Navone, N.M., et al. (2012). Modeling a lethal prostate cancer variant with small-cell carcinoma features. *Clin. Cancer Res.* *18*, 666–677.
- Ueda, T., Mawji, N.R., Bruchofsky, N., and Sadar, M.D. (2002). Ligand-independent activation of the androgen receptor by interleukin-6 and the role of steroid receptor coactivator-1 in prostate cancer cells. *J. Biol. Chem.* *277*, 38087–38094.
- Wan, X., Corn, P.G., Yang, J., Palanisamy, N., Starbuck, M.W., Efstathiou, E., Tapia, E.M., Zurita, A.J., Aparicio, A., Ravoori, M.K., et al. (2014). Prostate cancer cell-stromal cell crosstalk via FGFR1 mediates antitumor activity of dovitinib in bone metastases. *Sci. Transl. Med.* *6*, 252ra122.
- Wang, W., and Epstein, J.I. (2008). Small cell carcinoma of the prostate. A morphologic and immunohistochemical study of 95 cases. *Am. J. Surg. Pathol.* *32*, 65–71.
- Wu, Y.M., Su, F., Kalyana-Sundaram, S., Khazanov, N., Ateeq, B., Cao, X., Lonigro, R.J., Vats, P., Wang, R., Lin, S.F., et al. (2013). Identification of targetable FGFR gene fusions in diverse cancers. *Cancer Discov.* *3*, 636–647.
- Yang, L., Wang, L., Lin, H.K., Kan, P.Y., Xie, S., Tsai, M.Y., Wang, P.H., Chen, Y.T., and Chang, C. (2003). Interleukin-6 differentially regulates androgen receptor transactivation via PI3K-Akt, STAT3, and MAPK, three distinct signal pathways in prostate cancer cells. *Biochem. Biophys. Res. Commun.* *305*, 462–469.
- Zegarra-Moro, O.L., Schmidt, L.J., Huang, H., and Tindall, D.J. (2002). Disruption of androgen receptor function inhibits proliferation of androgen-refractory prostate cancer cells. *Cancer Res.* *62*, 1008–1013.
- Zhang, X.Q., Kondrikov, D., Yuan, T.C., Lin, F.F., Hansen, J., and Lin, M.F. (2003). Receptor protein tyrosine phosphatase alpha signaling is involved in androgen depletion-induced neuroendocrine differentiation of androgen-sensitive LNCaP human prostate cancer cells. *Oncogene* *22*, 6704–6716.
- Zou, M., Toivanen, R., Mitrofanova, A., Floc'h, N., Hayati, S., Sun, Y., Le Magnen, C., Chester, D., Mostaghel, E.A., Califano, A., et al. (2017). Transdifferentiation as a mechanism of treatment resistance in a mouse model of castration-resistant prostate cancer. *Cancer Discov.* *7*, 736–749.

## STAR★METHODS

## KEY RESOURCES TABLE

REAGENT or RESOURCE	SOURCE	IDENTIFIER
<b>Antibodies</b>		
Anti-AKT	Cell Signaling	Cat# 9272, RRID:AB_329827
Ant-Phospho-Akt (Ser473)	Cell Signaling	Cat# 4058, RRID:AB_331168
Anti-AR (N-20) antibody	Santa Cruz	Cat# sc-816, RRID:AB_1563391
Anti-Anti-MAP Kinase (ERK-1, ERK-2)	Sigma	Cat# M5670, RRID:AB_477216
Anti-Anti-MAP Kinase, Activated (Diphosphorylated ERK-1/2)	Sigma	Cat# M9692, RRID:AB_260729
Anti-FGF8 MAb	R&D Systems	Cat# MAB323, RRID:AB_2102956
Anti-Id1	Biocheck Inc.	Cat# 195-14; RRID: AB_115761
Anti-Anti-MAP Kinase (MEK 1/2)	Sigma	Cat# M5795, RRID:AB_260593
Anti-phospho-MEK1 (Ser298)	Millipore	Cat# 07-339, RRID:AB_310533
Anti-Prostate Specific Antigen	Dako	Cat# M0750, RRID:AB_2281105
Anti-Actin	Santa Cruz	Cat# sc-1616, RRID:AB_630836
Anti-Chromogranin A	Dako	Cat# M0869, RRID:AB_2081135
Anti-Synaptophysin	Dako	Cat# M0776, RRID:AB_2199013
Anti-Androgen Receptor	BioGenex	Cat# MU256-UC
Anti-Human Cytokeratin	Dako	Cat# M351501-2, RRID:AB_2631307
Anti-Synaptophysin	Santa Cruz	Cat# sc-17750, RRID:AB_628311
<b>Biological Samples</b>		
Patient-derived xenografts	University of Washington	LuCaP
Human localized and metastatic tumors	University of Washington Prostate Cancer Donor Autopsy Program	
<b>Chemicals, Peptides, and Recombinant Proteins</b>		
Power SYBR Green PCR Master Mix	ThermoFisher	Cat#4367659
DNeasy Blood & Tissue Kit	Qiagen	Cat#69506
Matrigel Matrix Growth Factor Reduced	BD Biosciences	Cat#354230
Teklad laboratory animal diets (doxycycline)	Envigo	Cat#td.04104
PD 173074	R & D Systems	Cat#3044/50
Ganciclovir	inVIVOgen	Cat#sud-gcv
MDV3100	Medivation Inc.	N/A
Recombinant Human/Mouse FGF-8b	R & D Systems	Cat#423-F8-025
Pierce Phosphatase Inhibitor Mini Tablets	ThermoFisher	Cat#88667
Pierce Protease Inhibitor Mini Tablets	ThermoFisher	Cat#88665
Goat anti-Rabbit IgG (H+L) Secondary Antibody	ThermoFisher	Cat#31460
Goat anti-Mouse IgG (H+L) Secondary Antibody	ThermoFisher	Cat#31430
SuperSignal West Pico Chemiluminescent Substrate	ThermoFisher	Cat#34087
Methyltrienolone (R1881)	Perkin Elmer	Cat#NLP005005mg
U0126	Cell Signaling Technology	Cat#9903
ESP3I	ThermoFisher	Cat#ER0451
RNeasy Plus Micro Kit	Qiagen	Cat#74034
TruSeq RNA Library Preparation Kit v2	Illumina	Cat#RS-122-2001
TruSeq Stranded mRNA Library Preparation Kit	Illumina	Cat# RS-122-2101
gentleMACS M Tubes	Miltenyi Biotec	Cat# 130-096-335
RNA STAT-60	Tel-Test	Cat# Cs-502

(Continued on next page)

**Continued**

REAGENT or RESOURCE	SOURCE	IDENTIFIER
<b>Critical Commercial Assays</b>		
CultreCoat Low BME Cell Invasion Assay, 96 well	R & D Systems	Cat#3481-096-K
CyQUANT Cell Proliferation Assay Kit	ThermoFisher	Cat#C7026
CellTiter-Glo Luminescent Cell Viability Assay	Promega	Cat#G7570
ApoLive Glo	Promega	Cat#G6411
<b>Deposited Data</b>		
Raw and analyzed Expression Microarray	<a href="#">Kumar et al., 2016</a>	GEO: GSE77930
Raw and analyzed aCGH Microarray Data	<a href="#">Kumar et al., 2016</a>	GEO: GSE77930
Expression microarray, aCGH Copy Number and Exome Sequencing Mutations MAF Data – FHCRC/ UW cohort	<a href="#">Kumar et al., 2016</a>	<a href="http://www.cbioportal.org/study?id=prad_fhcrc">http://www.cbioportal.org/study?id=prad_fhcrc</a>
Analyzed RNAseq data – SU2C cohort	<a href="#">Robinson et al., 2015</a>	<a href="http://www.cbioportal.org/study?id=prad_su2c_2015">http://www.cbioportal.org/study?id=prad_su2c_2015</a>
RNAseq data	This study	GEO: GSE99381
<b>Experimental Models: Cell Lines</b>		
LNCaP	ATCC	ATCC CRL-1740
LNCaP <sup>shAR</sup>	Laboratory of P.S. Rennie	<a href="#">Cheng et al., 2006</a>
LNCaP <sup>shAR/pATK</sup>	This Study	N/A
LNCaP <sup>APIPC</sup>	This Study	N/A
PacMetUT1	Laboratory of D.A. Troyer	<a href="#">Troyer et al., 2008</a>
PacMet AR-null #1, #2	This Study	N/A
22RV1	ATCC	CRL-2505
NCI-H660	ATCC	CRL-5813
<b>Experimental Models: Organisms/Strains</b>		
NOD- <i>scid</i> IL2Rgamma <sup>null</sup>	The Jackson Laboratory	005557
CB-17 SCID	Charles River	236
<b>Oligonucleotides</b>		
esiRNA targeting human <i>KIF11</i> CAUUGACAGUGGCCGAUAA	Sigma	Cat#SASI_Hs01_00161689
esiRNA targeting human <i>KIF11</i> CUGUACUACAGGAAUUGAU	Sigma	Cat#SASI_Hs01_00161696
esiRNA targeting human <i>KIF11</i> CAACAAGGAUGAAGUCUUAU	Sigma	Cat#SASI_Hs01_00161697
esiRNA targeting human <i>ID1</i> CCUCUCUGCACACCUACUA	Sigma	Cat#SASI_Hs01_00057899
esiRNA targeting human <i>ID1</i> GGGCGCUCCUCUCUGCACA	Sigma	Cat#SASI_Hs01_00246329
siRNA Targeting Human <i>FGF8</i> #1 CAAGAGCAACGGCAAAGGCAA	Qiagen	Cat#SI00145600
siRNA Targeting Human <i>FGF8</i> #2 GCGCUUCGAGUUCUCAACUA	Qiagen	Cat#SI02636725
siRNA Targeting Human <i>FGF9</i> #1 UUGGAUUAUACCUCCUAAUA	Qiagen	Cat#SI00031332
siRNA Targeting Human <i>FGF9</i> #2 CAGAGUCGGUUAGAGAGUAAA	Qiagen	Cat#SI04932011
sgRNA protospacer CTCCGGACCTTACGGGGACATG	This Paper	N/A
AR_Exon1_sgRNA+ caccgCTCCGGACCTTACGGGGACATG	This Paper	N/A
AR_Exon1_sgRNA- aaacCATGTCCCCGTAAGGTCCGGAGc	This Paper	N/A

(Continued on next page)

**Continued**

REAGENT or RESOURCE	SOURCE	IDENTIFIER
AR-fwd CRISPR verification primer CGACTTCACCGCACCTGATG	This Paper	N/A
AR-rev CRISPR verification primer AGGGCAGCAGCAGAAAATTAG	This Paper	N/A
qRT-PCR Primers	This Paper	Table S1
Recombinant DNA		
<i>HSV1-tk</i> gene in pORF vector	inVIVOgen	Cat#porf-hsv1tk
pATK	This paper	N/A
lentiCRISPRv2	Sanjana et al., 2014	Addgene Plasmid #52961
Software and Algorithms		
Prism v7	GraphPad	<a href="https://www.graphpad.com/scientific-software/prism/">https://www.graphpad.com/scientific-software/prism/</a>
TopHat v2.1.0	Kim et al., 2013	<a href="https://ccb.jhu.edu/software/tophat/index.shtml">https://ccb.jhu.edu/software/tophat/index.shtml</a>
Genomic Alignments v1.0.1	Lawrence et al., 2013	<a href="https://bioconductor.org/packages/release/bioc/html/GenomicAlignments.html">https://bioconductor.org/packages/release/bioc/html/GenomicAlignments.html</a>
edgeR v3.16.5	Robinson et al., 2010	<a href="https://bioconductor.org/packages/release/bioc/html/edgeR.html">https://bioconductor.org/packages/release/bioc/html/edgeR.html</a>
Ape v4.1	Paradis et al., 2004	<a href="https://cran.r-project.org/web/packages/ape/index.html">https://cran.r-project.org/web/packages/ape/index.html</a>
GSVA v1.24.0	Hänzelmann et al., 2013	<a href="https://bioconductor.org/packages/release/bioc/html/GSVA.html">https://bioconductor.org/packages/release/bioc/html/GSVA.html</a>
Scatterplot3d v0.3-40	Ligges and Machler, 2003	<a href="https://cran.r-project.org/web/packages/scatterplot3d/index.html">https://cran.r-project.org/web/packages/scatterplot3d/index.html</a>
GSEA v2.2.4	Subramanian et al., 2005	<a href="http://software.broadinstitute.org/gsea/index.jsp">http://software.broadinstitute.org/gsea/index.jsp</a>
MSigDB v6.0	Subramanian et al., 2005	<a href="http://software.broadinstitute.org/gsea/msigdb">http://software.broadinstitute.org/gsea/msigdb</a>
Other		
RNAiMax lipofectamine	ThermoFisher	Cat#13778030
Lipofectamine 2000	ThermoFisher	Cat#11668019
FBS Charcoal Dextran Stripped	Gemini Bio-Products	Cat#100-119

**LEAD CONTACT FOR REAGENT AND RESOURCE SHARING**

For further information and requests for reagents may be directed to and will be fulfilled by the corresponding author Peter S. Nelson ([pnelson@fredhutch.org](mailto:pnelson@fredhutch.org)).

**EXPERIMENTAL MODELS AND SUBJECT DETAILS****Cell Lines**

All cells were maintained at 37°C in a 5% CO<sub>2</sub> incubator. LNCaP (ATCC), 22RV1 (ATCC), and PacMet-UT1 (gift of D.A. Troyer) prostate cancer cell lines were grown in RPMI1640 (Invitrogen) supplemented with 10% FBS (Invitrogen) and 1% PenStrep (Invitrogen). NCI-H660 (ATCC) cells were grown in RPMI 1640 supplemented with 0.005 mg/ml insulin, 0.01 mg/ml transferrin, 30 nM sodium selenite, 10 nM hydrocortisone, 10 nM beta-estradiol, 4 mM L-glutamine, 5% FBS and 1% PenStrep. LNCaP<sup>shAR</sup> (gift of P.S. Rennie) were grown in RPMI1640 + 5%FBS + 1% PenStrep + 2.5 µg/mL Blasticidin (Invitrogen) + 1 µg/ml Puromycin (Invitrogen). LNCaP<sup>shAR/pATK</sup> (this study) were maintained in RPMI1640 + 5% FBS + 1% PenStrep + 2.5 µg/mL blasticidin + 1 µg/ml puromycin + 25 µg/ml Zeocin (Invitrogen). LNCAP<sup>APIPC</sup> (this study) were maintained in RPMI1640 + 5% CSS (Charcoal Dextran stripped FBS) (Gemini) + 1% PenStrep + 2.5 µg/mL blasticidin + 1 µg/ml puromycin + 25 µg/ml Zeocin + 1 µg/mL doxycycline (Clontech). Cell lines were authenticated by STR analysis by DDC Medical (Fairfield, OH).

**Tissue Acquisition**

Samples were obtained from male patients who died of metastatic CRPC and who signed written informed consent for a rapid autopsy performed within 8 hours of death, under the aegis of the Prostate Cancer Donor Program at the University of Washington. The Institutional Review Boards of the University of Washington and of the Fred Hutchinson Cancer Research Center approved this

study. LuCaP xenograft lines were established from specimens acquired at either radical prostatectomy or at autopsy, implanted, and maintained by serial passage in intact immune compromised male mice.

CRPC was assessed using immunohistochemical analysis to determine the distribution of adenocarcinoma (AR<sup>+</sup>), double-negative (AR<sup>-</sup>/NE<sup>-</sup>), and neuroendocrine (AR<sup>-</sup>/NE<sup>+</sup>) in these metastasis. Sites of metastases were ascribed a score between 0-200 for AR and SYP positivity. Any score <20 was categorized as negative to categorize each site.

### LNCaP<sup>APIPC</sup> Xenograft Mouse Models

NOD-scid IL2Rgamma<sup>null</sup> mice were purchased from the FHCRC animal facility. LNCaP<sup>APIPC</sup> cells were resuspended 1:1 in Matrigel (BD Biosciences) to a final concentration of 5x10<sup>6</sup> cells/ml and 100  $\mu$ l of cells were injected subcutaneously into the flank of castrated male mice. Xenografts were measured with digital calipers every 2 days and tumor volume was calculated using the formula  $(\pi/6)(L \times W^2)$ , where L is the length of the tumor and W its width. Animals implanted with LNCaP<sup>APIPC</sup> xenografts were maintained on a diet supplemented with doxycycline (200 mg/Kg, Harlan). When tumors reached a total volume of 200 mm<sup>3</sup> animals were enrolled into treatment arms consisting of PD173074 given at 50 mg/Kg/day by oral gavage five times per week or control vehicle 99% PBS with 1% DMSO used to dissolve PD173074. Each treatment group was composed of 8 animals. Animals were sacrificed when tumors reached a volume of 1500 mm<sup>3</sup>. All xenografts experiments were approved by the Fred Hutchinson Institutional Animal Care and Use Committee (File#1671).

### PDX Mouse Models

The LuCaP 173.2 patient-derived xenograft (PDX) line is from a rib metastasis obtained at time of death from a patient with CRPC and implanted into 6 week old immunocompromised male mice. CB-17 SCID mice (Charles River) were implanted subcutaneously with LuCaP 173.2 tumor tissue. Animals underwent rolling enrollment once tumors reached 100 mm<sup>3</sup> and were randomized into one of two groups (Control vs. Treatment). The FGFR inhibitor CH5183284 (Debio-1347) (Selleck chem) was dissolved in 100% DMSO and a 10-fold concentration of dosing solution was prepared. Then an equal volume of Cremophor EL was added to DMSO solution (5-fold concentration of dosing solution in 50 vol% DMSO/50 vol% Cr-EL). This solution was divided into daily usage amounts and stored at 4°C until each dosing day. For dosing, the stock solution was diluted with diluent (18.8 vol% PEG400 / 18.8% HPCD in distilled water) by 5-fold concentration on each day. The final concentration of vehicle was 10 vol% DMSO/10 vol% Cr-EL/15 vol% PEG 400/15% HPCD in distilled water as per [Nakanishi et al., 2014](#). LuCaP 173.2 tumor bearing animals received either vehicle (Control), while treated animals (Treatment) received 80 mg/kg CH5183284 4 days a week for 3.5 weeks via oral gavage. Note, 6 animals in the treated group received 100 mg/kg CH5183284 for 5 days/daily for one week before switching over to 80 mg/kg CH5183284 4 days a week due to loss of body weight. Tumor volumes (TV) were measured using digital calipers (calculated as  $(\pi/6)(L \times W^2)$ ) and body weights (BW) were measured twice weekly. Animals were euthanized after 3.5 weeks, when tumors exceeded 1,000 mm<sup>3</sup>, or when animals became otherwise compromised. The tumors were then divided equally into paraffin blocks with the remainder flash frozen for subsequent sequencing analysis. All PDX experiments were approved by the University of Washington Institutional Animal Care and Use Committee (File #2110-03).

## METHOD DETAILS

### Cell Culture

LNCaP<sup>shAR</sup> cells stably transfected with a tetracycline-inducible anti-AR shRNA, as previously described ([Cheng et al., 2006](#)), were obtained as a gift from Dr. Paul S. Rennie. These cells were further modified via Lipofectamine 2000 (Invitrogen) transfection of a plasmid encoding a triple-probasin-driven herpes thymidine kinase (HSV-TK) and a Zeocin resistance cassette. A clonal population of this cell line derived from Zeocin (Invitrogen) selection and serial dilution in a 96-well plate, which we refer to as LNCaP<sup>shAR/pATK</sup>, was subjected to total AR pathways suppression (TAPS): for two weeks the cells were grown in RPMI1640+5%CSS; at week 3, media was supplemented with 1 mg/mL doxycycline. Media was changed every 3-4 days and LNCaP<sup>shAR/pATK</sup> was maintained under TAPS for five months. A surviving colony of proliferating cells emerged. Following a 3-month expansion, this population of cells was treated with 50  $\mu$ M ganciclovir (GCV; InvivoGen) for two weeks to eliminate any cells still robustly expressing an AR transcriptional program. We referred to the surviving population as LNCaP<sup>APIPC</sup>.

### Migration and Invasion Assays

Migration and invasion assays were performed as per protocol in Cultrex 96-well cell invasion/migration transwell plates (R&D Systems). RPMI1640+/-10%FBS was added to the lower chamber and 100,000 cells suspended in serum-free RPMI1640 were added to the top chamber. For invasion assays, membranes were coated with 0.2x BME. Fluorescence was measured on a BioTek Synergy2 multiwell plate reader and normalized to LNCaP<sup>shAR/pATK</sup> RPMI1640 serum-free control.

### Cell Growth Assays

Cell growth was assayed by plating 5000 cells per well in a TC-treated 96-well black-sided, clear bottom plate (Corning). Media was changed every 48 hours and plates were collected at the reported timepoints and stored at -80°C. Plates for each experiment were assayed in batches using Cyquant (Invitrogen) to estimate cell viability as per manufacturer's protocol. Cells were treated with FGF8b

(25 ng/mL; eBioscience) or PD173074 (1  $\mu$ M; Tocris) or U0126 (25  $\mu$ M). Additionally, cells were treated with doxycycline (1 mg/mL) and enzalutamide (5  $\mu$ M) which was received as a gift from Medivation Inc.

Cells were plated as above and allowed to adhere for 24 hours then treated with various concentrations (as indicated in the figures) of CH-5183284 for 72 hours and assayed for apoptosis and viability using ApoLive Glo (Promega) following the manufacturer's instructions.

### Conditioned Media

Serum-free phenol red-free Optimem (Invitrogen) was added to 80% confluent LNCaP<sup>APIPC</sup> and LNCaP<sup>shAR/pATK</sup> cultured in a tissue culture-treated T75 flask (Corning). Twenty-four hours later, media was collected and centrifuged for 5 minutes at 5000 RPM to pellet cellular debris. The supernatant was added to an Amnicon Ultracel 3K centrifugal filter (Millipore) and concentrated as per manufacturer's instructions.

### siRNA Transfection

Cells were plated at 5000 cells/well in a 96-well plate in 100  $\mu$ l of phenol red-free Optimem supplemented with either 3% FBS or 3% CSS +1% PenStrep. Twenty-four hours after cell plating, cells were transfected with siRNA (Sigma) using RNAiMax lipofectamine reagent (Life Technologies) in 20  $\mu$ l total volume. Cell viability was estimated 96 hours after transfection by adding Cell Titer-Glo (Promega) and measuring luminescence (RLUs) as per protocol on a BioTek Synergy2 multiwell plate reader. Luminescence measurements from wells transfected with an equimolar pool of 3xKif11 siRNAs was used to estimate transfection efficiency. Transfections performed in 6-well plates for RNA collection used scaled-up conditions from 96-well experiments, and cells were harvested 24 hours after transfection as described below. siRNA sequences can be found in the [Key Resource Table](#).

### RNA Collection and Quantitative Real-Time PCR

Cell culture total RNA was isolated from 6-well plates using an RNEasy kit (Qiagen) as per protocol. qRT-PCR reactions were performed in triplicate using an Applied Biosystems 7900 sequence detector with SYBR Green PCR master mix (Invitrogen). Primers were designed using PrimerQuest (IDT, and all reactions were normalized to the expression of the housekeeping gene RPL13A. A water negative control did not produce significant amplification product. PCR primer sequences can be found in the [Table S1](#). Statistical analysis was performed using an unpaired two-sided Student's T-test to determine significance.

### Protein Collection and Immunoblotting

Protein was collected from tissue culture by lysing adherent cells with a cell lysis buffer (1.5 M Urea, 1% SDS, 1% NP-40, 2% Tween20, 250 nM NaCl, PBS) supplemented with 1x phosphatase inhibitors (PhosStop, Roche Diagnostics) and a 1x protease inhibitor cocktail (Complete Mini, Roche Diagnostics). Protein was quantified per protocol using a bicinchoninic acid assay (Thermo Scientific). Normalized cell lysates were loaded onto a 12% NuPAGE Bis-Tris gel (Invitrogen) in MES buffer. Protein was transferred to nitrocellulose membranes using a semi-dry transfer apparatus and Tris/CAPS buffer. Immunoblots were probed with primary antibodies targeting AKT (Cell Signaling), phospho-AKT (Ser473; Cell Signaling), AR (Santa Cruz), Erk1/2 (Sigma), diphosphorylated-Erk1/2 (Sigma), FGF8b (R&D Systems), ID1 (Biocheck, Inc.), MEK1/2 (Sigma), phospho-MEK1 (Ser298; Upstate), or PSA (Dako). Horseradish-peroxidase conjugated secondary antibodies (Thermo Scientific) were used in conjugation with Supersignal West Pico Chemiluminescent substrate (Thermo Scientific) to visualize protein targets. Membranes were then stripped for 15 minutes in Stripping Buffer (Thermo Scientific) and re-probed with anti-Actin antibody (Santa Cruz Biotechnology) as a loading control.

### Immunohistochemistry

PC metastases and xenograft tissues were fixed in buffered formalin (bone metastases were decalcified in 10% formic acid) and embedded in paraffin. Tissue microarrays (TMAs) were constructed using duplicate 1 mm diameter cores from these tissues. Five-micron thick sections of the TMAs were deparaffinized and rehydrated in sequential xylene and graded ethanol. Antigen retrieval was performed in 10 mM citrate buffer (pH 6.0) in a pressure cooker. Endogenous peroxidase and avidin/biotin were blocked respectively (Vector Laboratories Inc.). Sections were then incubated with 5% normal goat-horse-chicken serum, incubated with the following primary antibody dilutions: anti-Androgen Receptor (Biogenex) 1:60, anti-Prostate-specific Antigen (Dako) 1:1000, anti-Chromogranin A (Dako) 1:100, anti-Synaptophysin (Santa Cruz) 1:200 and anti-human cytokeratin (Dako) 1:100. They were subsequently incubated with biotinylated secondary antibody (Vector Laboratories Inc.), followed by ABC reagent (Vector Laboratories Inc.), and stable DAB (Invitrogen Corp.). All sections were lightly counterstained with hematoxylin and mounted with Cytoseal XYL (Richard Allan Scientific). Mouse or rabbit IgG were used as negative controls.

### AR CRISPR-Cas9 Editing

To create the sgRNA targeting exon 1 of AR, an sgRNA protospacer of CTCCGGACCTTACGGGGACATG was cloned in to the ESP31 enzyme (Thermo Fisher) sites of the lentivirus expression vector lentiCRISPRv2 (Addgene Plasmid #52961) using annealed oligos and AR\_Exon1\_sgRNA+: caccgCTCCGGACCTTACGGGGACATG and AR\_Exon1\_sgRNA-: aaacCATGTCCCCGTAAGGTCCGGAGc. To confirm on-target cutting, cells were transfected with lentiCRISPRv2:AR-sgRNA or GFP control using lipofectamine 2000 (Thermo Fisher) according to manufacturer's recommendation. After five days of selection with 1.5  $\mu$ g/mL puromycin, genomic DNA was isolated using the DNeasy Blood & Tissue Kit (Qiagen) and amplified using Phusion High-Fidelity DNA Polymerase (New England

Biolabs) and primers: AR-fwd CGACTTCACCGCACCTGATG and AR-rev AGGGCACGCAGCAGAAATTAG. On target CRISPR cutting was confirmed using T7 endonuclease I (New England Biolabs) heteroduplex cleavage assay to measure insertion/deletions, introduced via NHEJ-mediated double strand break repair of CRISPR activity.

PacMetUT1 cells were seeded in 10 cm dishes and transfected with lentiCRISPRv2:AR-sgRNA using lipofectamine 2000 (Thermo Fisher) according to manufacturer's protocols and recommendations. Cells were supplemented with 25 ng/mL FGF8b (R&D Systems) or PBS + 0.1% human BSA solvent control during five days of selection with 1.5  $\mu$ g/mL puromycin. The surviving cells were replaced with fresh medium (RPMI 1640 10% FBS with or without FGF8b) and allowed to grow into colonies. Medium was changed once a week and FGF8b was replenished every three days. Approximately 5 weeks later, colonies were isolated from both FGF8b and PBS/BSA supplemented cells and allowed to expand for further analyses. Two colonies from cells treated with FGF8b were confirmed to be AR-negative by Western blot (GeneTex). These two colonies were referred to as the AR-null #1 and AR-null #2 sublines.

### Transcript Profiling Methods

Cell line RNA was extracted using the Qiagen RNeasy Kit, (Qiagen Inc.), according to the manufacturer's protocol. On-column DNase digestion was performed. CRPC metastases RNA samples were prepared by reviewing a H&E of the frozen tissue block, followed by scoring the block with a razor so as to have as pure as possible sections of tumor. Cores were obtained from each of the bone metastases frozen tissue blocks that had been previously identified based upon review of H&E sections from corresponding paraffin embedded blocks; adjacent areas of tumor were cored out of the frozen tissue blocks using a 2 mm diameter tissue punch in a  $-20^{\circ}\text{C}$  cryostat. Cores were homogenized in gentleMACS M Tubes (Miltenyi Biotec). Tissues were then isolated with RNA STAT-60 (Tel-Test). RNA concentration, purity, and integrity was assessed by NanoDrop (Thermo Fisher) and Agilent Bioanalyzer. Cell line RNA-seq libraries were constructed from 1  $\mu$ g total RNA using the Illumina TruSeq RNA Library Prep Kit v2 according to the manufacturer's protocol. CRPC Metastases RNA-seq libraries were constructed from 1  $\mu$ g total RNA using the Illumina TruSeq Stranded mRNA Library Prep Kit according to the manufacturer's protocol. Barcoded libraries were pooled and sequenced on the Illumina HiSeq 2500 generating 50 bp paired end reads. Sequencing reads were mapped to the hg19 human genome using TopHat v2.1.0. Gene level abundance was quantitated from the filtered human alignments in R using the Genomic Alignments v1.0.1 Bioconductor package.

### QUANTIFICATION AND STATISTICAL ANALYSIS

Student's T-test was used to comparable significance between grouped quantitative data sets using GraphPad Prism 7.0 software. Differences were considered significant if  $p \leq 0.05$ . Differences in tumor volume (TV) between control and treated animals were calculated using unpaired t-tests with unequal variances, with significance set at  $p \leq 0.05$ .

Differential expression was assessed using transcript abundances as inputs to the edgeR v3.16.5 Bioconductor package in R. FDR and fold-change thresholds for significance are listed in the figure legends.

Unsupervised clustering of cell line expression profiles was performed in R on the 1000 most variable genes (calculated as the inter-quartile range of the  $\log_2$  transcripts per million reads) using Euclidean distance and average-linkage. Clusters were visualized using the ape v4.1 Cran package.

The gene expression signature activity scores were calculated in R using the GSVA v1.24.0 Bioconductor package, using  $\log_2$  transcripts per million reads as input. Pearson's correlation coefficient was used to study the relationships between variables shown in scatterplots using the cor.test function in R. The scatterplot3d v0.3-40 Cran package was used to plot three dimensional scatterplots.

Gene expression group comparisons were ranked by edgeR statistics and used to conduct Gene Set Enrichment Analysis using the GSEA v2.2.4 software to determine patterns of pathway activation in different phenotypic groups. We used the curated pathways and gene sets within MSigDBv6.0.

Genome-wide comparisons of copy number between DNPC and ARPC groups was performed using two-tailed fisher's exact tests using the fisher.test function in R. Proportions of tumors with somatic copy number alterations were compared, including high (greater than 1 copy) gain or homozygous loss.

### DATA AND SOFTWARE AVAILABILITY

The RNA sequencing data has been deposited at the Gene Expression Omnibus (GEO) site: <https://www.ncbi.nlm.nih.gov/geo/> under accession number GSE99381.